[American Journal of Science, Vol. 317, June, 2017, P. 641–676, DOI 10.2475/06.2017.01]

American Journal of Science

JUNE 2017

A MODEL FOR THE DECREASE IN AMPLITUDE OF CARBON ISOTOPE EXCURSIONS ACROSS THE PHANEROZOIC

AVIV BACHAN*,†, KIMBERLY V. LAU*,+, MATTHEW R. SALTZMAN**, ELLEN THOMAS***, LEE R. KUMP§, and JONATHAN L. PAYNE*

ABSTRACT. The geological cycling of carbon ties together the ocean-atmosphere carbon pool, Earth's biosphere, and Earth's sedimentary reservoirs. Perturbations to this coupled system are recorded in the carbon-isotopic ($\delta^{13}C$) composition of marine carbonates. Large amplitude $\delta^{13}C$ excursions are typically treated as individual events and interpreted accordingly. However, a recent compilation of Phanerozoic carbon isotopic data reveals that $\delta^{13}C$ excursions are a ubiquitous feature of the geologic record, and thus should be considered in concert. Analysis indicates that Phanerozoic carbon isotope excursions, as a whole, have characteristic durations of 0.5 to 10 M.yr. and exhibit declining amplitude over time. These commonalities suggest a shared underlying control.

Here we demonstrate that sinusoidal modulation of the sensitivity of organic carbon and phosphate burial in a simple numerical model of the geologic carbon cycle results in large, asymmetric $\delta^{13}C$ oscillations that exhibit their largest amplitudes in the 0.5 to 10 M.yr. period range. As anoxia is known to strongly modulate the C:P burial ratio of organic matter in sediments, we propose that sea-level oscillations were the primary source of sinusoidal modulation for the geologic carbon cycle, and that their degree of influence on the carbon cycle was determined by the state of oxygenation of bottom waters overlying the continental shelves. When oxygen minimum zones (OMZs) were large, shallow, and prone to expansion, sea-level changes would have had the capacity to drive large changes in the areal extent of OMZs in contact with the sea-floor, resulting in strong leverage on the burial sensitivity of organic carbon and phosphate, and thus on $\delta^{13}C$. Progressive oxygenation of the oceans, which was facilitated by biological innovations, resulted in a decline in the amplitude of $\delta^{13}C$ excursions over the Phanerozoic, and the biogeochemical stabilization of the Earth System.

Key words: carbon cycle, carbon isotopes, marine carbonates, global biogeochemical cycles, linear systems

INTRODUCTION

Phanerozoic Carbon Isotope Data

Over the past 60 years, carbon isotope ratios measured in marine carbonates and organic matter have been a key tool for deriving insights into past climate and ocean chemistry. Over these decades, the trend has been one of ever increasing temporal resolution of carbon isotopic data, evolving hand in hand with ever more refined

* Department of Geological Sciences, Stanford University, 450 Serra Mall, Building 320, Stanford, California 93405
** School of Earth Sciences, The Ohio State University, 125 South Oval Mall, Columbus, Ohio 43214
*** Geology and Geophysics Department, Yale University, New Haven, Connecticut 06520
§ Dept. of Geosciences, The Pennsylvania State University, 503 Deike Building, University Park, Pennsylvania 16802
+ Current address: Department of Earth Sciences, University of California, Riverside, Geology Building, Riverside, California 92521
† Corresponding author: avivbd@stanford.edu; aviv.bachan@gmail.com

insights into carbon cycle dynamics. Craig (1953) carried out a survey of terrestrial materials and meteorites, and demonstrated that the isotopic ratios of organic carbon and carbonate carbon align with their estimated fractions within the total crustal carbon pool based on geological observations (Clarke, 1924). In the 1970s and '80s Phanerozoic trends were first determined. It was shown that Phanerozoic $\delta^{13}C$ values increased to a mid-Paleozoic high and then decreased to the present, and that this trend was matched by an inverse trend in sulfate $\delta^{34}S$ (Veizer and others, 1980; Kump and Garrels, 1986; Holser, 1988). These sets of isotopic data then served as inputs for a series of carbon cycle models that grew progressively in their sophistication. Developed in the '80s and '90s, these models were aimed at reconstructing the histories of atmospheric O_2 and CO_2 over the Phanerozoic (Berner and others, 1983; Garrels and Lerman, 1984; Lasaga and others, 1985; Kump and Garrels, 1986; Berner, 1987; Berner and Canfield, 1989; Lasaga, 1989; Berner, 1991; Kump, 1993; Berner, 1994; Berner, 2001; Berner and Kothavala, 2001; Berner, 2006). Beginning in the 1980s, analysis of carbon isotope ratios via mass spectrometry became sufficiently routine that the measurement of hundreds or even thousands of samples became feasible, opening the door to detailed characterization of individual stratigraphic sections and high-resolution chemostratigraphy among sections. First carried out in the Cretaceous (Scholle and Arthur, 1980), and later in many other time intervals (Knoll and others, 1986; Magaritz, 1989; Payne and others, 2004; Saltzman, 2005; Halverson and others, 2005; Maloof and others, 2010), these highly resolved carbon isotopic records revealed numerous large-amplitude excursions in the $\delta^{13}C$ of marine carbonates. Many of these excursions have been related to geologic events including extinctions (Payne and others, 2004; Bachan and others, 2012), climate perturbations (Zachos and others, 2001), sea-level changes (Cramer and Saltzman, 2007), and volcanic eruptions (Svensen and others, 2004, 2007, 2009).

Recently, a sufficient number of these individual high-resolution records have become available, providing sufficient coverage of the Phanerozoic, such that a view of carbonate $\delta^{13}C$ at sub-million-year resolution over the entirety of the Phanerozoic can now be realized (fig. 1, Appendix table A1, Saltzman and Thomas, 2012). The composite curve reveals that the majority of Phanerozoic $\delta^{13}C$ variation consists not of noise (as it had previously appeared in lower-resolution data compilations: for example, Veizer and others, 1999), but rather of stratigraphically coherent positive and negative excursions. The improved resolution allows for partitioning of the data via spectral decomposition. Figure 2 shows the results of a three-fold partitioning: (A) a first-order long-term trend with a period that is the same duration as the length of the time series (542 M.yr.), (B) second-order variations with periods of 10s to 100s of M.yr., and (C) third-order variations with periods of 0.5 to 10 M.yr. The results show that excursions with the largest amplitudes all have durations of less than 10 M.yr., and show declining amplitude over time. This interpretation is further supported by examination of the data in the frequency domain. Figure 3 shows the spectrum of the data, with two levels of smoothing applied (red and blue dots). Also shown is the slope of a random walk (green line). The overall shape of the signal is sigmoidal, but variations with periods of 3 to 6 M.yr. show excess power. In addition, as the timescale of variations decreases, the lower portion of the spectrum (periods of less than 3 M.yr.) increasingly is dominated by noise. Temporal trends in frequency can be seen in a plot of frequency over time (spectrogram), albeit at the cost of decreased frequency resolution. Figure 4A shows the filtered signal containing only second and third-order components (spanning 0.5–270.5 M.yr.) and figure 4B shows the spectrum of the signal over time. The decline in the power of higher frequencies is evident, as is the periodic nature of the changes in the width of the signal envelope. These periodic changes in the envelope are highlighted in figure 5C, and are plotted alongside other

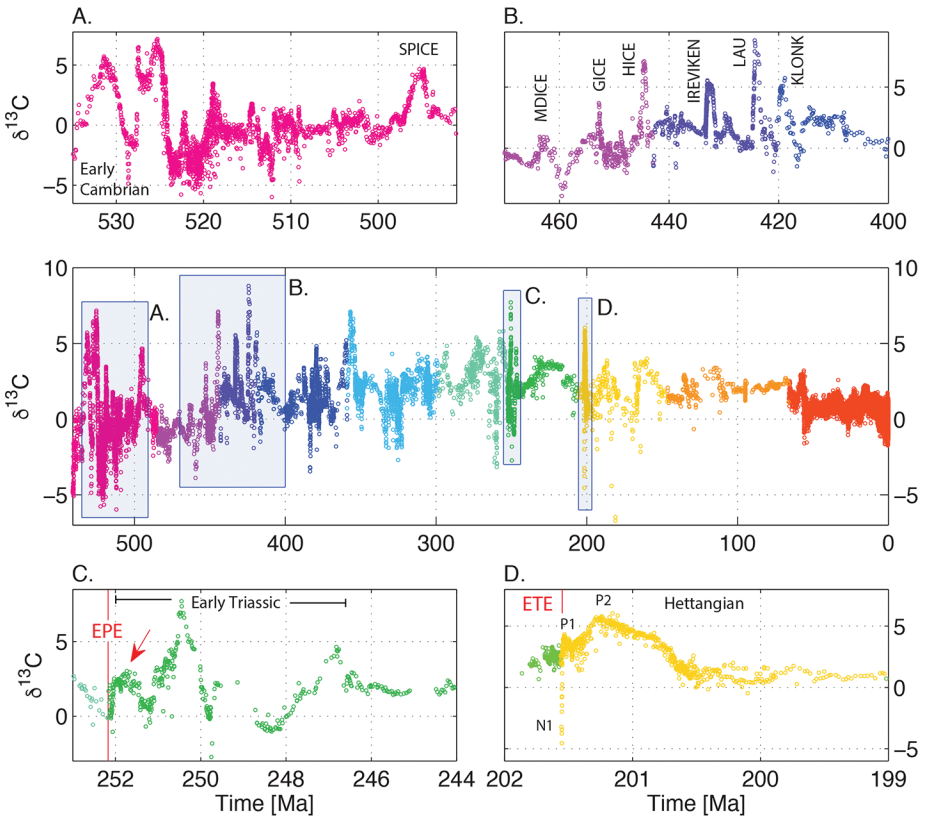

Fig. 1. The Phanerozoic carbon isotope record colored according to period. Note that the observed variability about the mean largely consists of stratigraphically coherent and well-resolved positive and negative excursions in $\delta^{13}C$, whose amplitudes generally decrease through time. Panels A–D show intervals of interest. (A) Early Cambrian. (B) Late Ordovician, Silurian, and early Devonian. (C) End-Permian mass extinction (EPE, red line) and Early Triassic carbon cycle oscillations. Arrow marks first positive excursion after the EPE. (D) End-Triassic mass extinction (ETE, red line) and the N1, P1, and P2 carbon isotope excursions, which together comprise the Hettangian carbon cycle instability. The ETE occurs coincidentally with the N1 excursion, and the P1 is the first positive excursion following the ETE. Data replotted from Saltzman and Thomas, (2012) with addition of data from Bachan and others, (2012).

records that have been postulated to vary periodically with similar periods (~50 M.yr.): (A) global diversity of short-lived genera (Rohde and Muller, 2005), and (B) area of preserved marine strata in North America during the Phanerozoic (green) together with a 55 M.yr. oscillatory component extracted using singular spectrum analysis (red, Meyers and Peters, 2011). Also shown are North American sequences (Sloss, 1963; Peters, 2008).

Interpretation of Phanerozoic Carbon Isotope Data

The canonical interpretation of carbon isotope data in marine carbonates is that long-term trends (much greater than the 100 k.yr. residence time of carbon in the ocean-atmosphere system) reflect the balance between the input of carbon and its burial as carbonate sediments and organic matter (Kump, 1991; Hayes and others, 1999). This interpretation is supported by a few key observations. First, the long-term $\delta^{13}C$ trend over the Phanerozoic (fig. 2A) as measured in bulk carbonates is largely replicated in well-preserved fossils with pristine features (Veizer and others, 1999). This correspondence suggests that the long-term trend is not likely to have been

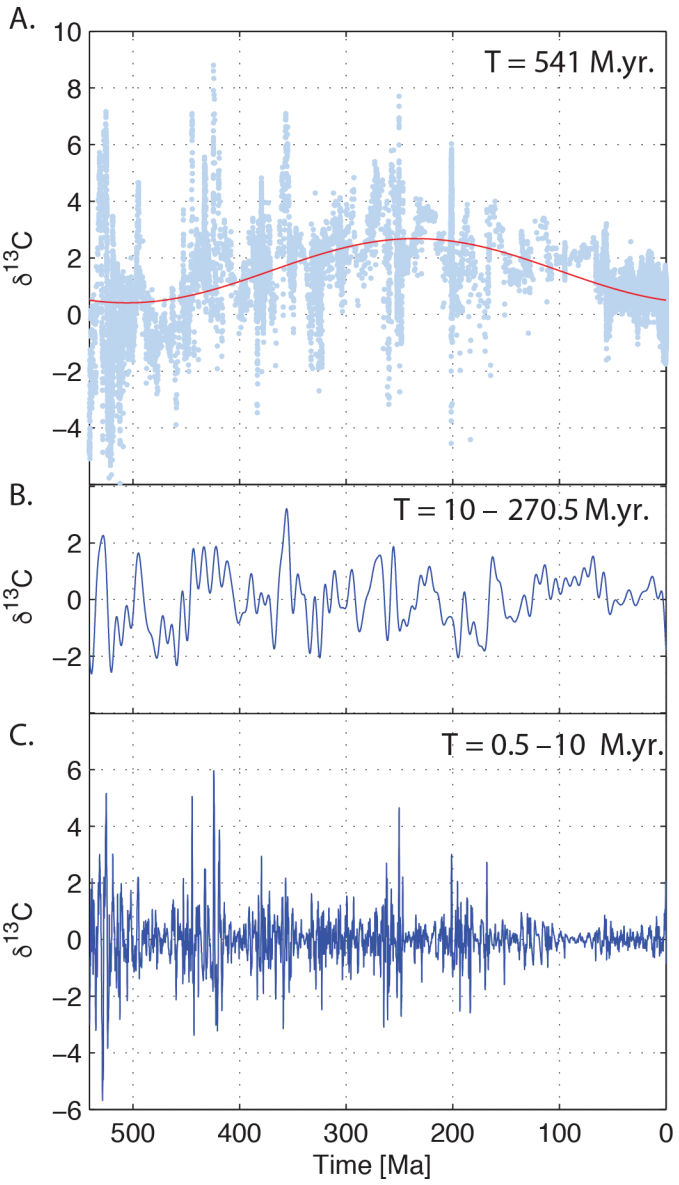

Fig. 2. Spectral decomposition of the Phanerozoic $\delta^{13}C$ curve. (A) First-order (541 M.yr.) trend (red line) and raw data (light blue dots). (B) Second order trends with periods spanning 10–270.5 M.yr. (C) Variation with periods spanning the 0.5–10 M.yr. range. Note that the largest excursions are in the 0.5–10 M.yr. range. See also appendix fig. A1.

strongly modified by diagenesis, and that it is largely representative of the average $\delta^{13}C$ of dissolved inorganic carbon in seawater. Second, the inverse correlation between the stable isotopic systems of carbon and sulfur affirms that the long-term trends in $\delta^{13}C$ are predominantly due to variations in the burial fraction of organic carbon that was produced by oxygenic photosynthesis, and not by the burial of other ^{13}C-depleted phases such as authigenic carbonate or organic carbon derived from anoxygenic

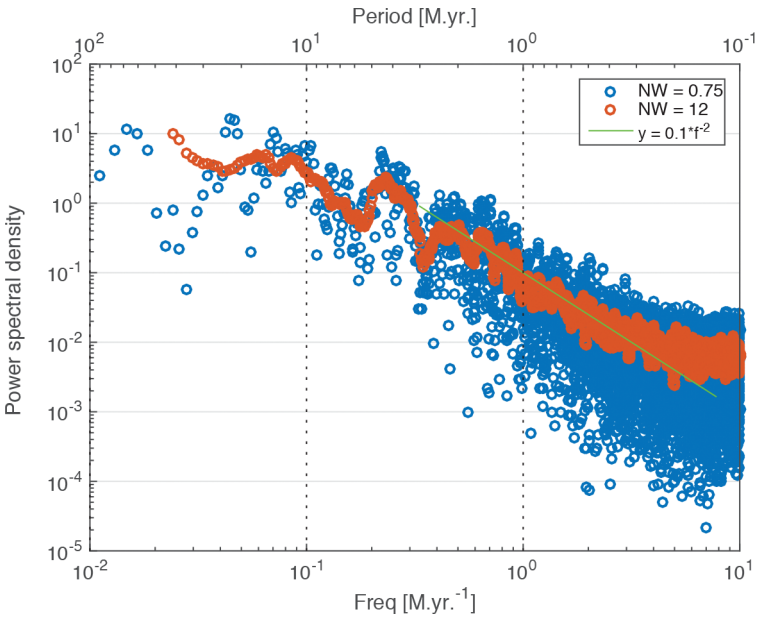

Fig. 3. Spectrum of Phanerozoic $\delta^{13}C$ data obtained via a Thompson power spectral density estimate, with two levels of smoothing applied (blue and red points). Also shown is the slope of a random walk (green line). Note the peak in power between periods of 3–6 M.yr.

photosynthesis. This confirmation is due to the fact that the burial of organic carbon (which leads to ^{13}C enrichment) is the only process associated with O_2 release. The released O_2 leads to increased oxidation of sulfides that are ^{34}S-poor, resulting in inversely correlated trends in carbonate $\delta^{13}C$ and sulfate $\delta^{34}S$ (Garrels and Perry, 1974;

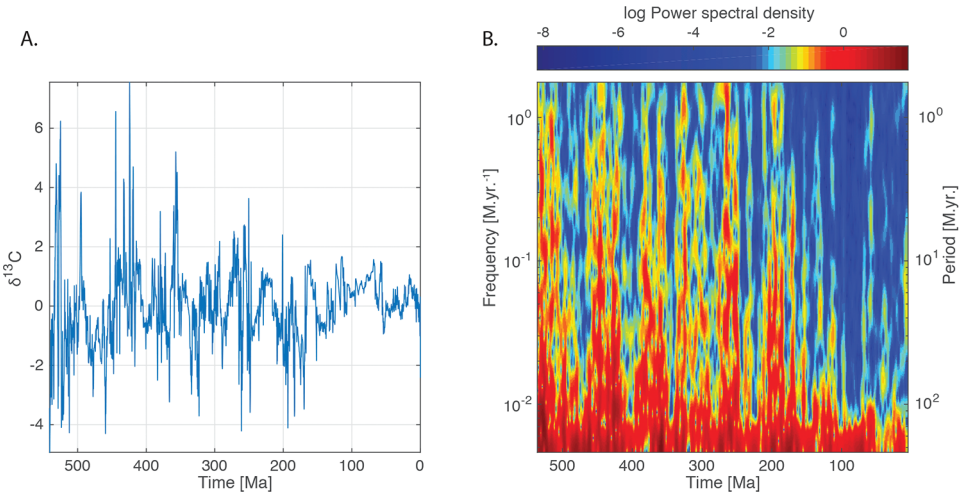

Fig. 4. A. Filtered signal containing only second and third-order components (270.5–0.5 M.yr.). B. Spectrogram of the filtered signal. The periodic nature of the changes in the variance of the signal are evident, as is the decline in power of higher frequencies from the mid-Mesozoic onward.

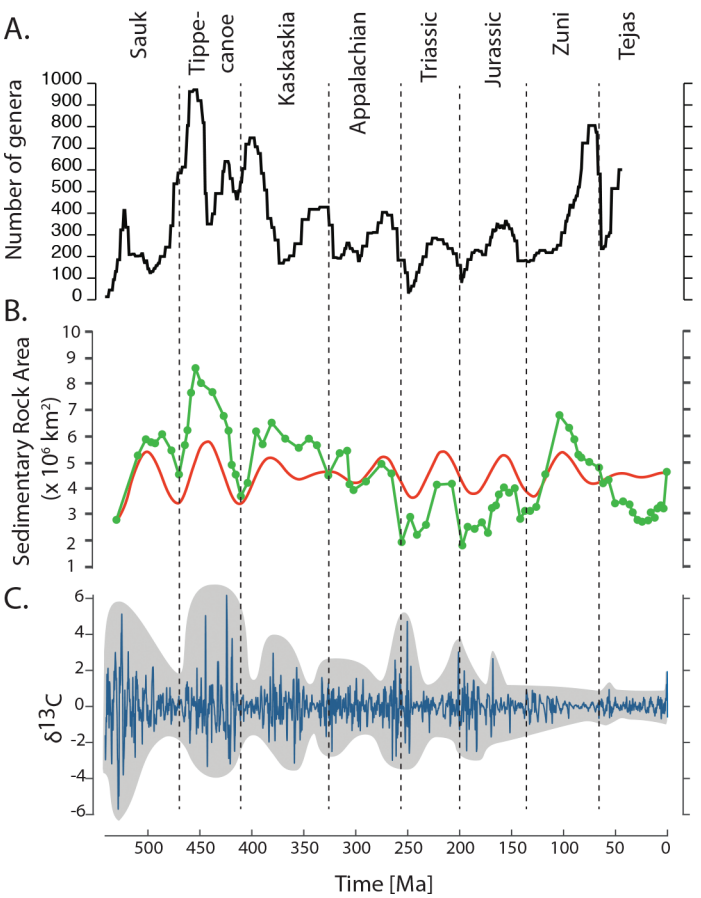

Fig. 5. Periodic changes in the envelope of third-order $\delta^{13}C$ variations (0.5–10 M.yr.) plotted alongside other records that have been postulated to vary periodically with similar periods (~50 M.yr.). (A) Global diversity of short-lived genera (Rohde and Muller, 2005). (B) Area of preserved marine strata in North America during the Phanerozoic (green) and a 55 Myr oscillatory component extracted using singular spectrum analysis (red, Meyers and Peters, 2011). (C) Variations on the 0.5–10 M.yr. timescale with the envelope of variability highlighted in gray. Also shown are North American sequences (dashed lines, Sloss, 1963; Peters, 2008). Note decline in coherence from the Paleozoic to the post-Paleozoic.

Veizer and others, 1980; Kump, 1993). Third, the $\delta^{13}C$ trend correlates with independent estimates of sedimentary volume and biotic diversity (Hannisdal and Peters, 2011). This correlation is difficult to account for through diagenesis, and points toward a shared tectonic driver.

Do $\delta^{13}C$ excursions and variations occurring on shorter timescales (0.5–10 M.yr.) similarly represent the average isotopic composition of the ocean-atmosphere carbon pool? There are a number of arguments that support a positive answer to this question. Many—though not all—$\delta^{13}C$ excursions in carbonate rocks occur also in coeval organic matter (Knoll and others, 1986; Bachan and others, 2012; Meyer and others, 2013), suggesting that variations in $\delta^{13}C$ existed in the original water column. Furthermore, many excursions can be correlated across widely separated stratigraphic locations and shown to be synchronous, suggesting widespread regional—if not global—distributions (Gale and others, 1993; Husson and others, 2016). The common association of carbon isotope excursions with extinctions (Magaritz, 1989), sea-level

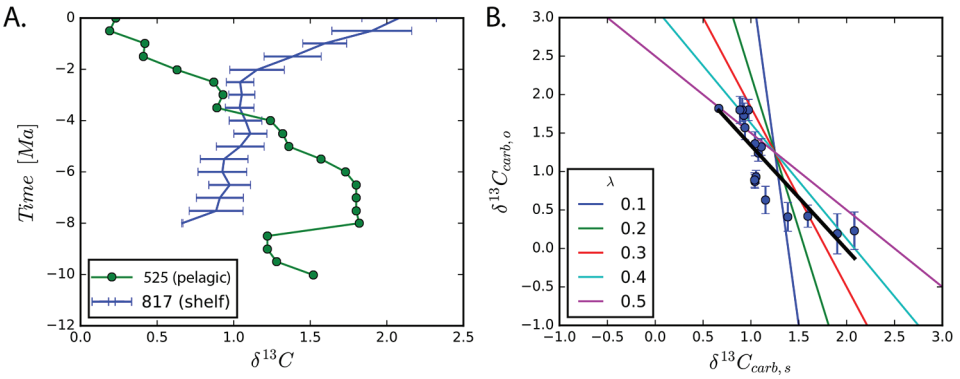

Fig. 6. (A) Data from Swart, (2008) showing trends in global $\delta^{13}C$ as recorded by pelagic carbonates (site 525) contrasted with those exhibited by a peri-platform site (site 817). (B) Cross-plot of shelf and pelagic data together with best-fit line (black), and model estimates for a two end-member carbonate burial flux with different proportions of shelf and pelagic sinks. Best-fit line is sub-parallel to 0.4–0.5 model lines indicating that shelf carbonate consist of approximately 50% of the total carbonate sink, which is consistent with estimates based on geologic data (Milliman, 1993).

changes (Cramer and Saltzman, 2007), anoxia (Scholle and Arthur, 1980) and, in the Mesozoic and Paleogene in particular, evidence for widespread volcanism (Svensen and others, 2004; Svensen and others, 2007), further suggests that trends in the $\delta^{13}C$ record most likely reflect global perturbations to ocean-atmosphere carbon pool.

Yet this interpretation of carbon isotope excursions has been challenged by observations of modern and recent carbonate deposits that indicate that shelf carbonates—the chief component of the carbonate rock record in deep time—show trends that are very different than those known to characterize the global carbon cycle (Swart and Eberli, 2005; Swart, 2008; Gischler and others, 2009). Moreover, in shallow-water platform sections, carbon isotope trends not dictated by secular seawater variation show covariance between organic carbon and carbonate carbon (Oehlert and Swart, 2014). And, in both platform and periplatform sites these trends are shared among widely separated stratigraphic locations—possibly coupled through sea level (Swart and Kennedy, 2012). The causes of these trends are still debated, and may arise from local restriction, water-mass aging, and biotic influences on the $\delta^{13}C$ of carbonate produced on platform tops, open system diagenesis and flushing of shelf carbonates with sea-water and/or meteoric waters, alteration during neomorphism of aragonite to calcite, admixture of aragonite derived from platform tops with pelagically derived material, or some combination of these factors.

Yet, although the trends observed in periplatform sites are different than the pelagic record, they are not uncorrelated with it. Many of the periplatform sites detailed in these studies (Swart and Eberli, 2005; Swart, 2008) show a clear inverse correlation with open ocean $\delta^{13}C$ (fig. 6A). It is possible that this correspondence is coincidental. It is also possible that the "unbalanced" burial of ^{13}C-enriched carbonates (that is, without corresponding burial of organic carbon) on the shelves drove down the $\delta^{13}C$ value of pelagic carbonates resulting in an inverse correlation between the two burial fluxes of carbonate. This hypothesis can be articulated quantitatively by modification of the canonical expression for carbon isotope steady-state behavior to include the existence of two carbonate sinks:

$$\delta^{13}C_{volc} = \delta^{13}C_{carb} - \varepsilon f_{\mathrm{org}} \quad (1)$$

$$\delta^{13}C_{carb} = \delta^{13}C_{carb,s} *(1 - \lambda) + \delta^{13}C_{carb,o} *(\lambda) \quad (2)$$

$$\delta^{13}C_{carb,o} = \frac{\delta^{13}C_{volc} + f_{org}\varepsilon - \delta^{13}C_{carb,s} * (1 - \lambda)}{\lambda} \quad (3)$$

Equation (1) is the canonical expression relating $\delta^{13}C$ of the ocean-atmosphere system ($\delta^{13}C_{carb}$) to the fraction of organic carbon burial (f_{org}), the isotopic value of the volcanic/weathering input of carbon ($\delta^{13}C_{volc}$), and the fractionation imparted by photosynthesis (ε). Equation (2) parses the overall carbonate burial flux into a shelf sink and an "other" sink. Equation (3) is the result of substituting (2) into (3) and isolating $\delta^{13}C_{carb,o}$. Figure 6B shows the model predictions for various values of the partitioning between the shelf and "other" carbonate sinks (using values of −5‰, 25‰ and 0.25 for $\delta^{13}C_{volc}$, ε, and f_{org}, respectively), alongside data from Swart (2008). The slope of the best-fit line to the data (solid black line) is subparallel to the 0.4–0.5 model lines, suggesting that roughly half of carbonate burial occurs on the shelf while the rest occurs in the pelagic realm. This partitioning calculated from isotope ratios is in agreement with independent estimates drawn from geologic data (Milliman, 1993).

From a deep-time standpoint, the "Bahamas" mode of carbon cycle operation (globally correlated local controls on $\delta^{13}C$) is perfectly permissible. Yet, it is unlikely to have been very prevalent in the geologic past. First, in portions of the Mesozoic in which pelagic carbonates are abundant, the shelf and pelagic records show generally similar trends (Grötsch and others, 1998; Parente and others, 2007; Vincent and others, 2010), rather than inversely correlated trends. Thus, the behavior of carbonate platform and periplatform sediments on the shelves over the last 10 M.yr. must be unique or limited to ice-house intervals. Second, without a volumetrically significant second carbonate sink (pelagic or otherwise) mass balance would limit the extent to which large $\delta^{13}C$ variations in shallow-marine carbonates could vary independently of the $\delta^{13}C$ of the ocean-atmosphere carbon pool. That is, even if synchronized through sea-level changes and/or ocean chemistry, shallow marine carbonates with $\delta^{13}C$ values substantially different than the $\delta^{13}C$ value of the global carbon pool must have remained limited in volume if they were not to have impacted the isotopic composition of the global pool. Without an additional carbonate sink, widespread "unbalanced" burial of ^{13}C-enriched carbonates on the shelves would be expected to result in a decline in the $\delta^{13}C$ value of the ocean-atmosphere pool over a few hundred k.yr., which would cause the isotopic composition of the isotopically deviant carbonate flux to promptly return to the equilibrium value demanded by global mass balance. Such mass balance constraints are expected to be more stringent in a world without a pelagic carbonate sink, such as existed prior to the mid-Mesozoic (Boss and Wilkinson, 1991). Third, if $\delta^{13}C$ variation in shelf limestones arises primarily due to local or regional factors, such as physical restriction and segregation from well-mixed open ocean water, with inter-regional correlation imposed by sea-level changes, then such variation should be prevalent whenever sediment reflecting similar conditions is sampled in the geologic record. Yet, Cretaceous shallow-marine carbonates are as widespread, shallow, and intensively sampled as Paleozoic shallow-marine carbonates, but do not show the same large excursions (Jenkyns, 1995; Erba and others, 1999; Price and others, 2016, fig. 1). This striking difference in isotopic character between otherwise similar facies suggests that the differences between the pre and post mid-Mesozoic are not likely to simply be a consequence of sampling a better-preserved carbonate record, but rather indicate a fundamental shift in the operation of the Earth system over time.

The canonical interpretation of carbon isotope data has been further challenged in other ways. Carbonation of basalts (Bjerrum and Canfield, 2004) and the precipitation of authigenic carbonate in sediments (Higgins and others, 2009; Schrag and others, 2013; Sun and Turchyn, 2014) have been proposed as under-appreciated carbonate sinks that may have been much larger in the past. Yet, to accommodate the

mass balance constraints these sinks would have to have been of similar size to the shelf carbonate sink, or strongly fractionated from sea-water. To date, the evidence that has been supplied has been anecdotal (Shibuya and others, 2012; Greene and others, 2012; Saitoh and others, 2015; Thomazo and others, 2016, Zhou and others, 2016; Cui and others, 2017), and vast quantities of isotopically depleted authigenic carbonate have not been reported in Phanerozoic strata or in other periods. Thus, we must await a comprehensive survey of these sinks in ancient sediments to evaluate their importance. Nonetheless, even if true, these alternative formulations still share many features with the traditional interpretation. Though organic carbon is postulated not to be the primary ^{13}C-depleted phase that is removed from the surficial system, both of these alternative formulations are still global in character, and both hypotheses still rely on respiration of organic matter to sustain δ^{13}C gradients in the ocean (for carbonated basalts) or in the sediment (for authigenic carbonate precipitation), and are thus not decoupled from the fate of organic carbon in the ocean. Consequently, even if large, strongly fractionated sinks for carbonate waxed and waned through geologic time, they likely did so in response to ocean chemistry and other geologic events (see for example, Greene and others, 2012; Cui and others, 2017).

If the shelf carbonate record indeed represents global carbon cycle dynamics, then a number of pertinent questions arise: Why do δ^{13}C excursions decline in amplitude over the Phanerozoic? Why do they have characteristic durations of 0.5 to 10 M.yr.? And why do δ^{13}C excursions show a correspondence with sea-level changes, extinctions, volcanism, and anoxia? In the following we develop a hypothesis to explain these oft-observed correlations (which might be named the "harmonic" hypothesis for carbon cycle operation). It is predicated on a face-value reading of the carbon isotope record, and pre-supposes that δ^{13}C excursions in carbonate sediments reflect variations in global ocean chemistry occurring at the time of their deposition.

UNDERSTANDING OSCILLATIONS OF THE GEOLOGIC CARBON CYCLE

Model Formulation

Many sophisticated models have been put forth to interpret geochemical records and simulate global biogeochemical dynamics (BLAG, Berner and others, 1983; COPSE, Bergman and others, 2004; MAGic, Arvidson and others, 2006). The goal here is not to replicate these models. Rather, our goal is to produce the *simplest* possible model that still bears a semblance of the physical system being modeled, and can produce results that are qualitatively similar to the carbon isotope record. The model (fig. 7) includes only two reservoirs: oceanic phosphate (M_P) and carbon in the ocean-atmosphere system (M_C). Phosphate enters the ocean through the weathering of phosphate-bearing rocks (F_{wp}) and exits through precipitation and burial of phosphate-bearing phases (F_{bp}). Carbon enters the ocean-atmosphere system through an input flux (F_{in}) comprising volcanism (F_v), the weathering of carbonate carbon (F_{wc}), and the weathering of organic carbon (F_{wo}). Carbon exits through the burial of carbonate (F_{bc}) and organic carbon (F_{bo}). We follow Kump and Arthur (1999) in balancing alkalinity by setting carbonate burial to the sum of silicate weathering (F_{ws}) and carbonate weathering: $F_{bc} = F_{wc} + F_{ws}$. The model equations are thus:

$$\begin{aligned} \frac{dM_P}{dt} &= F_{wp} - F_{bp} \\ \frac{dM_C}{dt} &= F_v + F_{wo} - F_{ws} - F_{bo} \end{aligned} \tag{4}$$

The functional forms of the dependencies of the fluxes on the reservoirs are formulated to align as best as possible with our understanding of biogeochemical

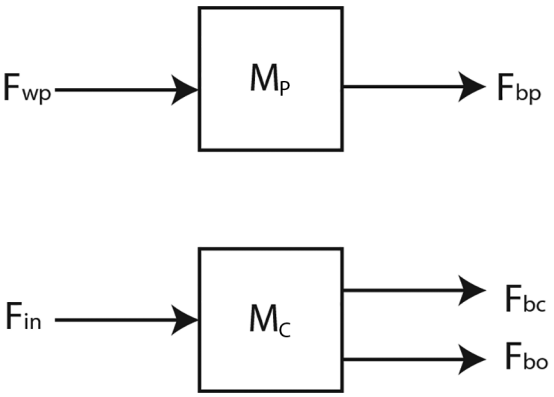

Fig. 7. A simple model of the coupled cycles of oceanic phosphate and ocean- atmosphere carbon over geologic timescales.

dynamics while still maintaining model simplicity. Consider the burial flux of organic carbon and its dependence on the phosphate reservoir. Phosphate is a biolimiting nutrient in the ocean and on land and its availability (alongside those of nitrogen and iron) is critical in determining organic productivity (Sarmiento and Gruber, 2006). This dependence of organic productivity on phosphate availability impacts organic carbon burial over geological time scales (Broecker, 1971; Van Cappellen and Ingall, 1996). Organisms extract phosphate from the surface ocean with nearly complete scavenging efficiency (Broecker, 1971). The phosphate is incorporated into their biomass at a ratio of 1:106 with carbon (Redfield, 1958). Most of the organic carbon is decomposed in the water column, and the carbon and phosphate are remineralized. A small fraction of the organic matter that is produced in the surface ocean makes its way to the sediments. There, the fates of the carbon and phosphate bound within the organic matter diverge: some of the phosphate is released back into the water column while the carbon is retained, resulting in elevated C:P ratios of buried organic carbon relative to the Redfield ratio (Froelich and others, 1982). Under an anoxic water column C:P burial ratios tend to be even higher. This is because the cap of iron oxides that usually keeps any phosphate that is remineralized in the sediments trapped within them is removed, resulting in an efflux of phosphate from the sediments into the water column. Once in place, the release of phosphate from sediments can result in increased productivity, which may drive further anoxia, resulting in an anoxia-productivity feedback (Van Cappellen and Ingall, 1996). Thus, one could consider the burial rate of organic carbon as dependent on the burial rate of phosphate from the ocean into the sediments multiplied by a C:P burial ratio of those sediments (which may be strongly redox dependent). We assume that the burial flux of phosphate is dependent on oceanic phosphate concentrations ($F_{bp} = k_{bp}*M_P$), so a dependence of organic carbon burial on the mass of phosphate in the ocean arises as well ($F_{bo} = C/P*k_{bp}*M_P = k_{bo}*M_P$). Alternatively, at a constant preservation rate, increased phosphate availability leads to increased organic productivity and increased organic carbon burial, such that one similarly ends up with a dependence on the mass of oceanic phosphate. Either way, the dependencies of organic carbon and phosphate burial on phosphate availability encapsulate within them the efficiency with which organic carbon and phosphate are exported from the surface ocean to the sediments, as well as the efficiency with which they are preserved in the sediments relative to each other.

While the burial of phosphate is dependent on marine processes, its delivery is terrestrially sourced and weathering-dependent, and hence related to pCO_2 and to the mass of carbon in the ocean-atmosphere system. At a given level of calcium in the ocean, pCO_2 is expected to vary as the square of the mass of carbon in the ocean (Kump and Arthur, 1999). Weathering rates scale as a function of the 0.3 to 0.6 power of the CO_2 level (Walker and others, 1981). Together these relationships result in a near linear dependence of P delivery on the mass of carbon in the ocean ($F_{wp} = k_{wp}*M_C$). Silicate weathering is expected to behave in a similar way to phosphate weathering, and so carbonate burial (or at least the component of the carbonate burial flux that is derived from silicate weathering) is expected to scale with the mass of carbon in the ocean-atmosphere system ($F_{ws} = k_{ws}*M_C$). By substituting the burial flux of carbonate with the sum of silicate and carbonate weathering we assume immediate compensation of imbalances in alkalinity. For Phanerozoic times, compensation occurs on timescales of ~ 0.1 M.yr. (Hönisch and others, 2012) so this assumption is not likely to be grossly violated. Testing the impact of including separate formulations for inputs and outputs of alkalinity is left for future model exploration. Additionally, we treat organic carbon weathering as an invariant source of carbon similar to volcanism. Organic carbon weathering likely depends on atmospheric oxygen in non-linear ways (Chang and Berner, 1999; Lasaga and Ohmoto, 2002; Wildman and others, 2004; Bolton and others, 2006), as do the burial efficiencies of phosphate and organic carbon (Laakso and Schrag, 2014). Incorporating of the impact of varying atmospheric pO_2 on model fluxes is left for future model improvement.

The functional dependencies of the fluxes on the reservoirs are likely to be non-linear globally (that is, over their entire range). However, for small perturbations about the long-term Phanerozoic steady-state, the flux behaviors should be tolerably approximated by a first-order (linear) dependence. Under such a linear parameterization, in which each flux is the product of a reservoir and a coefficient ($F_j = k_j*M_j$), the model takes the following form:

$$\begin{aligned} \frac{dM_P}{dt} &= k_{wp}M_C - k_{bp}M_P \\ \frac{dM_C}{dt} &= F_v + F_{wo} - k_{ws}M_C - k_{bo}M_P \end{aligned} \tag{5}$$

Note that under this formulation of the model, both the burial flux of organic carbon and the weathering of phosphate respond to reservoirs *other* than the ones to which they are directly connected, while the burial fluxes of carbonate and phosphate are directly related to the carbon and phosphate reservoirs, respectively. Because the model is linear, these equations can be cast in matrix notation:

$$\begin{bmatrix} \dot{M}_P \\ \dot{M}_C \end{bmatrix} = \begin{bmatrix} -k_{bp} & k_{wp} \\ -k_{bo} & -k_{ws} \end{bmatrix} \begin{bmatrix} M_P \\ M_C \end{bmatrix} + \begin{bmatrix} 0 \\ F_v + F_{wo} \end{bmatrix} \tag{6}$$

The model can then be expressed more compactly, where arrows indicate vectors and underlining indicate matrices:

$$\dot{\vec{M}} = \underline{K}\vec{M} + \vec{F} \tag{7}$$

The advantage of assuming a linear system and applying matrix notation is that a closed-form solution exists for the time evolution of the system, and it is similar in form to the familiar solution for a scalar case. The time evolution of the system following perturbations from steady-state is then given by:

$$\vec{M}(t) = \vec{M}^{ss} + e^{\underline{K}t}(\vec{M}(0) - M^{ss}) \tag{8}$$

Equation 8 states that deviations from steady-state ($M(0) - M^{ss}$) will evolve exponentially with time, at a rate determined by the coefficient matrix $\underline{K}$, where similarly to the scalar case ($M = F/k$), the steady-state values are determined by the balance between the long-term (quasi-constant) inputs and outputs (see Appendix table A2 for flux values):

$$M^{ss} = -\underline{K}^{-1}\vec{F}_{in} \tag{9}$$

In particular, the temporal evolution of the system is determined by the eigenvalues of the coefficient matrix. By applying an eigenvalue decomposition to the coefficient matrix (Lasaga, 1980), the solution can be expressed as a sum of terms, each consisting of an initial value coefficient (a_i) and an eigenvector (v_i) multiplied by an exponential holding the corresponding eigenvalue (λ_i):

$$\vec{M}(t) = \vec{M}^{ss} + a_1\vec{v}_1e^{\lambda_1 t} + a_2\vec{v}_2e^{\lambda_2 t} + \cdots \tag{10}$$

In general, the eigenvalues can be complex numbers with real and imaginary components. The real part determines the rate of decay (or growth) and the imaginary part controls oscillations. Past work (Southam and Hay, 1976; Lasaga, 1980, 1981) generally assumed that geochemical systems would be over-damped. Here we obtain the eigenvalues analytically (see Appendix for calculation and for comparison to a mass-spring system), and derive an explicit condition for oscillations:

$$\kappa = \frac{4k_{wp}k_{bo}}{(k_{bp} - k_{ws})^2} \tag{11}$$

The parameter κ determines the degree to which the model response will be oscillatory. When $\kappa > 1$, the system will respond in an oscillatory manner to an impulsive perturbation. When $\kappa < 1$, the system will return via smooth exponential decay to its pre-perturbation value. When $\kappa = 1$, the return will be most rapid. By analogy to a mass spring system, the coupled positive and negative feedbacks provided by the cross terms (organic carbon burial and phosphate delivery) act like the restoring force of a spring, whereas the direct terms (phosphate burial and silicate weathering) act like friction. When the feedbacks associated with the cross-terms are sufficiently strong, the system will oscillate.

Numerical Results

To investigate the model's behavior, we perturb it in two ways. First, to obtain the model's response to an instantaneous perturbation (impulse response) we perturb the model with a quasi-instantaneous input of carbon and examine its response at three values of κ (fig. 8). Second, to obtain the model's response to a sinusoidal forcing (frequency response) we perturb the model with a sinusoidal forcing spanning a range of frequencies and amplitudes (fig. 9). We apply idealized forcing functions, rather than real-world forcings, as doing so has the advantage of giving a general model response that is independent of the particulars of the input. Further, although the system is linear in mass, and therefore the propensity for mass oscillations can be determined analytically, it is non-linear with respect to $\delta^{13}C$ because isotopic mass involves the product of mass and isotopic composition ($M \times \delta$). Consequently, numerical integration is required to investigate the model's $\delta^{13}C$ response.

In the three cases of instantaneous carbon release (fig. 8), we perturb the model with an injection of carbon equivalent to 50 percent of the C reservoir size (1.9×10^{18} mol). The injected carbon is assigned a $\delta^{13}C$ value equal to that of the volcanic input (-5 ‰). The first run (fig. 8A, blue line) is carried out using accepted estimates for

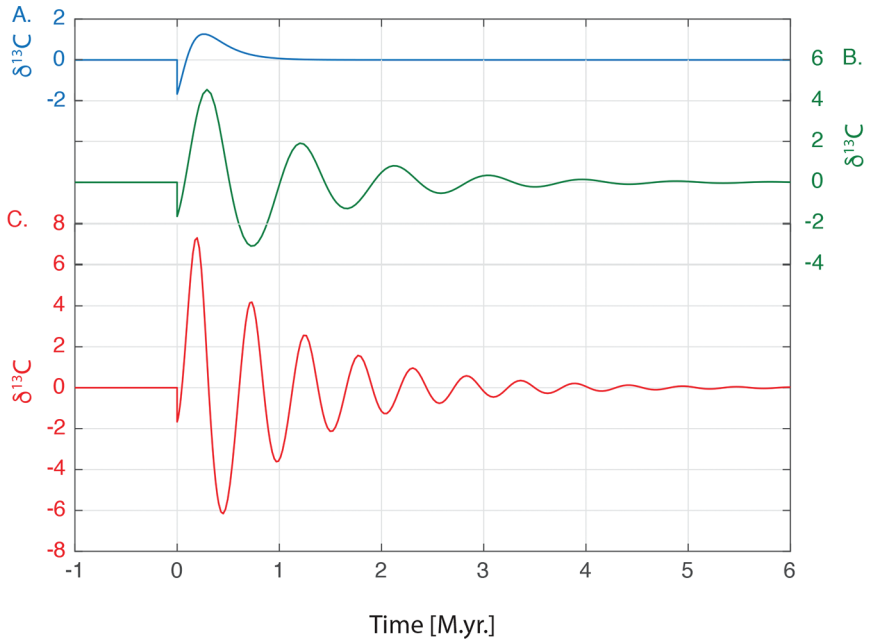

Fig. 8. Model response to an instantaneous 50% addition of carbon to the C reservoir. (A) Model parameters set to average Phanerozoic values (κ = 3.4). (B) As in (A), but with the burial dependence of phosphate (k_{bp}) and the weathering dependence of silicates (k_{ws}) each set to 1/10 of their default values (κ = 340). (C) As in (B), but with the burial sensitivity of organic carbon (k_{bo}) set to three times its default value (κ = 1020). Total run duration is 6 M.yr. With decreasing magnitude of the direct terms (k_{bp} and k_{ws}) and increasing magnitude of the cross terms (k_{wp} and k_{bo}) the $\delta^{13}C$ response becomes more oscillatory and decays more slowly.

the average Phanerozoic flux magnitudes and reservoir sizes (Kump and Arthur, 1999, see Appendix table A2 for values). We find that in its natural state the system is not entirely damped, and the release of carbon drives increased weathering resulting in increased input of phosphate, increased organic carbon burial, and a small positive excursion following the negative one. This slight under-damping is reflected in a value of κ that is larger than unity: κ = 3.4. In the second run (fig. 8B, green line), the burial dependence of phosphate (k_{bp}) and the weathering dependence of silicates (k_{ws}) are each set to $1/10^{th}$ of their default values, corresponding to κ = 340. The interaction between the M_P and M_C reservoirs is now more pronounced and results in multiple excursions from a single perturbation. In the third run (fig. 8C, red line), in addition to the conditions in the second run, the burial sensitivity of organic carbon (k_{bo}) is set to three times its default value, corresponding to κ = 1020. The progressive increase in κ results in a progressive increase in the frequency and amplitude of oscillations. Note that in all cases the largest overshoot in the positive direction immediately follows the negative excursion resulting from the pulse of carbon input.

We approach the sinusoidal forcing through two different formulations. The first is by prescribing that the flux to which the perturbation is applied vary sinusoidally with a given amplitude (A) and frequency (ω). This formulation is reasonable for external fluxes such as the volcanic flux, but not for fluxes such as organic carbon burial that are presumed to be strongly dependent on the size of their respective reservoirs. Thus, we employ a second formulation in which we force the fluxes sinusoidally while retaining their dependence on their respective reservoir size. In the

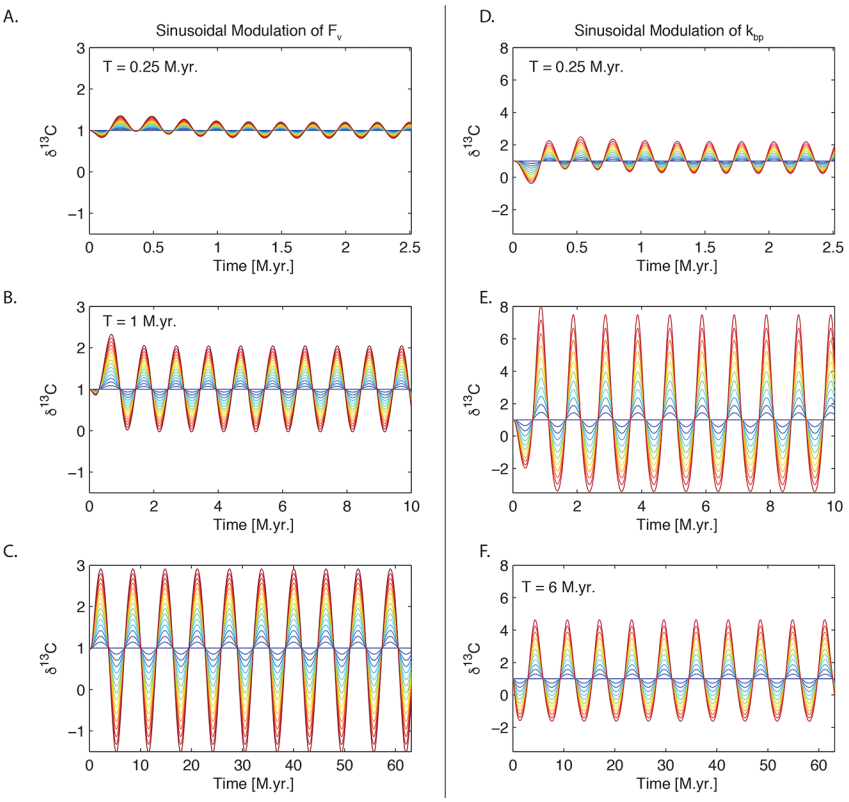

Fig. 9. (A) Model $\delta^{13}C$ response to sinusoidal modulation of volcanic input (F_v), and (B) P burial when indirectly forced (k_{bp}). The maximal amplitude of the forcing is constant among the three runs, but its period is progressively longer: 0.25 M.yr., 1 M.yr., and 6 M.yr. Sinusoidal forcing of the volcanic input results in a progressively increasing amplitude of response with increasing period, whereas for P burial the amplitude of the resulting $\delta^{13}C$ oscillations is largest when the period of the forcing is approximately 1 M.yr. Color denotes amplitude of forcing (see fig 10 for colorbar): maximal amplitude shown for Fv is 0.6, and for kbp is 0.44. See appendix figs. A2-A–A2-C for all model parameters.

first case, the flux being forced can be written as $F = F_0 + A \sin \omega t$, where F_0 is the base value of the flux. In the second case, the flux being forced can be written as $F = kM(1+A \sin \omega t) = k'(t)M$, where k is the flux rate dependence and M is the corresponding reservoir. In the first case, the flux becomes constant when the amplitude of the forcing is zero, whereas in the second case the expression returns to the unperturbed parameterization when the amplitude of the forcing is zero. This difference in formulation is subtle yet leads to a significant difference in interpretation. In the first case, the sinusoidal forcing completely replaces the original parameterization of the flux, so the flux varies sinusoidally with the prescribed amplitude and frequency without regard to reservoir size. Whereas, in the second case, it is the dependence of the flux on the reservoir size (rather than the flux itself) that varies sinusoidally with prescribed amplitude and frequency. For instance, under the second formulation, the burial sensitivity of organic carbon on phosphate would vary with time: at times a given amount of phosphate would generate a certain burial flux of organic carbon, while at other times a much larger burial flux would result. In other words, the dependence of organic carbon burial on phosphate is forced to vary sinusoidally, and this forcing results in sinusoidal modulation of the organic carbon

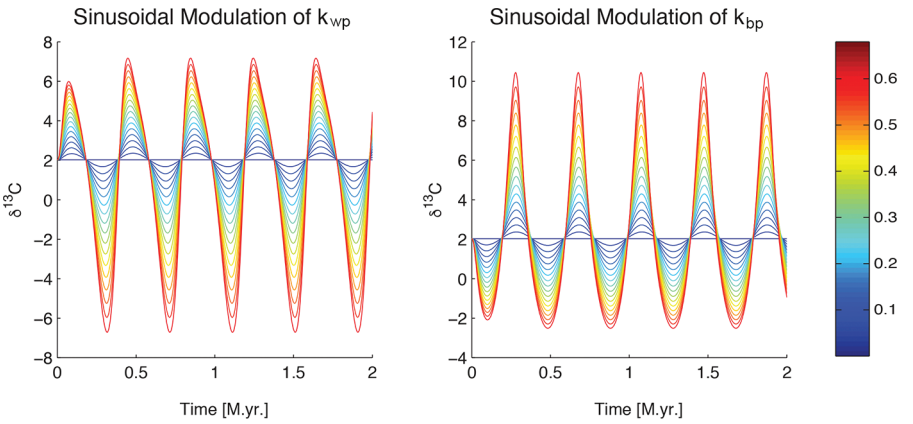

Fig. 10. Example of asymmetric model $\delta^{13}C$ output in response to symmetric sinusoidal forcing. Colorbar denotes amplitude of the forcing, as in fig 9. See figs. A2-A–A2-C for all model parameters.

burial flux. Further, the amplitude parameter (A) can be viewed as representing the sensitivity of the rate parameter (k) to an external forcing whose amplitude we consider fixed. A large value of A would indicate a stronger coupling, while a small value of A would indicate a weaker coupling. In the first case, where the fluxes are modulated directly, we denote the result with the name of the flux (for example, F_v, F_{ws}, . . .). In the second case, where the rate coefficients are modulated, we denote the runs with the name of the coefficient (for example, k_{ws}, k_{bp}, . . .). In the first case, the system is non-linear in $\delta^{13}C$. But in the second case, it is much more strongly so: in addition to the non-linearity inherent in isotopic mass balance, the rate coefficients now vary sinusoidally with time.

We explore the impact of varying the period of the forcing on the model $\delta^{13}C$ response by running the model iteratively with periods spanning 0.01 M.yr. to 1000 M.yr. (Appendix figs. A2-A to A2-C). We also vary the amplitudes between 0 (no forcing) to 1 (doubling of the steady-state value of the flux/parameter). In general, increasing the amplitude of the forcing results in larger $\delta^{13}C$ oscillations (fig. 9). However, at a given amplitude of the forcing, the period of the forcing affects the amplitude of the resulting $\delta^{13}C$ oscillations. In some cases, the model exhibits a progressively increasing amplitude with increasing period of the forcing (figs. 9A–9C), whereas in others the model exhibits a maximal response at between periods of approximately 0.5 to 10 M.yr., and more muted responses higher and lower periods (figs. 9D–9F). The occurrence of a resonant peak is not predicted by classical linear systems theory: the eigenvalues of the system have not changed. Rather, this behavior arises due to the non-linearity imposed on the system by the sinusoidal modulation. The observed result of non-symmetric output (fig. 10) in response to a symmetric forcing is also not predicted by classical theory. The asymmetry includes both large negative excursions separated by smaller right-skewed positive excursions, as well as large positive excursions separated by smaller negative excursions (fig. 10). These asymmetric excursions can reach very large amplitudes without violating mass balance constraints (that is, resulting in negative mass). Indirect forcing of the burial flux of phosphate (k_{bp}) with a period of 1 M.yr. (fig. A2-A) results in positive excursions up to +25 permil under the maximal modulation explored (A = 1). On the longest timescales simulated (T = 100 M.yr) indirect forcing of organic carbon burial and phosphate weathering (k_{wp} and k_{borg}) results in positive intervals lasting 50 M.yr. separated by large (up to −20 ‰) negative excursions (fig. A2-C). These negative

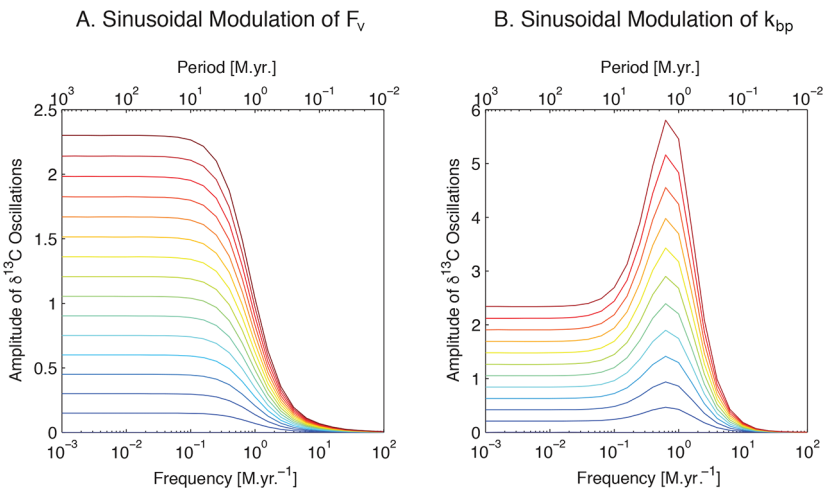

Fig. 11. Plot of the amplitude of model $\delta^{13}C$ response as a function of the frequency of the forcing for: (A) volcanic input; and (B) P burial when forced indirectly (same as fig. 9). The two responses are representative of the range of model responses. Some fluxes exhibit a sigmoidal shaped response, while others show a resonant peak in the 0.5–10 M.yr. periods. See also fig. A3. Color denotes amplitude of forcing; maximal amplitude values as in figure 9. Note that the amplitude of $\delta^{13}C$ oscillations referred to in this figure equals half of the $\delta^{13}C$ range in the time domain.

excursions are driven by nearly pure organic carbon weathering. Periodic $\delta^{13}C$ excursions with such amplitude and frequency do not occur in the Phanerozoic, but characterize the Neoproterozoic (Halverson and others, 2005) and possibly the Paleoproterozoic (Sekine and others, 2010).

The two different types of frequency responses shown by the model can be more clearly evaluated when the amplitude of the $\delta^{13}C$ response is plotted as a function of the frequency/period of the forcing (figs. 11A, 11B and Appendix fig. A3). A sigmoidal frequency response is exhibited by model parameters and fluxes with a progressive increase in the amplitude of $\delta^{13}C$ oscillations with increasing period (fig. 11A), whereas model parameters that are particularly sensitive to the forcing within a certain range of frequencies exhibit a resonant peak (fig. 11B). Of the nine parameters investigated (Appendix fig. A3), five show a sigmoidal frequency response, whereas four show a resonant peak between periods of 0.5 and 10 M.yr.: the weathering sensitivity of phosphate (k_{wp}), the burial dependence of phosphate (k_{bp}), the burial dependence of organic carbon (k_{bo}), and the burial flux of phosphate when forced directly (F_{bp}). The weathering of phosphate (k_{wp}) and the burial of organic carbon (k_{bo}) show a second, broad, resonant peak over the longest periods investigated (100 to 1000 M.yr.).

DISCUSSION

Implications of Model Results for Phanerozoic $\delta^{13}C$ Trends

In principle, a number of end-member scenarios can account for the duration and amplitude of individual $\delta^{13}C$ excursions as well as the decline in their amplitude over the Phanerozoic. First, the geologic carbon cycle may be strongly non-linear (Wallmann, 2014) or inherently oscillatory (Zachos and Kump, 2005), so that, under certain conditions, it might have the capacity to produce regular variations in $\delta^{13}C$ without requiring external forcings, or be only weakly dependent on them. Second, variations in $\delta^{13}C$ could directly reflect variations in the strength and timing of the physical

forcings that drive $\delta^{13}C$ excursions. Third, $\delta^{13}C$ variations could reflect the dynamics of external forcings as well as the sensitivity of the carbon cycle to those forcings. Under the first scenario, internal carbon cycle dynamics would account for both the timing and magnitude of individual excursions, as well as the general decline in the amplitudes of excursions over the Phanerozoic. Under the second scenario, both these attributes would be a result of changes in the amplitude of external physical forcings. Under the third scenario, the $\delta^{13}C$ record would be a product of an external pacemaker and an internal carbon cycle amplifier. The three scenarios correspond in a general sense to the three modeling scenarios: impulse forcing (fig. 8), direct sinusoidal forcing (fig. 11A), and indirect sinusoidal forcing (fig. 11B), respectively.

A number of lines of evidence suggest that internally generated oscillations are not likely to be a source of repeated $\delta^{13}C$ excursions in the Phanerozoic carbon isotopic record (or at least not in response to impulsive perturbations). First, given estimated average Phanerozoic values for reservoir sizes and flux magnitudes, the model predicts an oscillatory ($\kappa_0 = 3.4$) yet highly damped response. Order-of-magnitude modification of flux dependencies (from $\kappa = 3.4$ to $\kappa = 1020$) is required to produce multiple oscillations in response to a single forcing impulsive perturbation. Such a large increase in κ would have to have been driven by very large reductions in the kinetics of precipitation of carbonate and phosphate. It is not clear whether such large changes can be realistically attributed to secular variation in the mode of carbonate and phosphate precipitation over the Phanerozoic.

Perhaps more problematically, the model predicts that the largest peak in $\delta^{13}C$ should immediately follow the negative excursion associated with injection of carbon. This prediction is not met in at least two cases where the timing and duration of volcanism relative to the carbon isotopic record are reasonably well constrained (Blackburn and others, 2013; Burgess and Bowring, 2015). Both the Early Triassic (following the end-Permian mass extinction, fig. 1C) and the Early Jurassic (following the end-Triassic mass extinction, fig. 1D) are characterized by multiple $\delta^{13}C$ excursions (Payne and others, 2004; Bachan and others, 2012). In both cases, the largest peak is separated from the initial negative excursion by a smaller positive peak (the first positive following the EPE is marked with an arrow in fig. 1C and the first positive following the ETE is marked by the "P1" annotation in fig. 1D). In both cases, the largest peak (most positive $\delta^{13}C$ excursion) lags the initial volcanically-driven negative excursion substantially (>1.3 M.yr., and ~500 k.yr., respectively). Model modifications cannot easily account for the lag: the sensitivity of organic carbon burial in the model must be reduced to nearly zero immediately following carbon injection in order to see peak organic carbon burial lag peak carbon injection. Yet, geochemical proxies suggest that conditions expected to promote organic carbon burial, including anoxia (Lau and others, 2016), and increased delivery of sediment due to an intense weathering regime (Algeo and Twitchett, 2010) rise to their maximal extent immediately following the end-Permian extinction event. Taken in aggregate, these observations suggest that it is unlikely that the multiple $\delta^{13}C$ excursions in either the end-Permian or end-Triassic records were internally generated. Other factors must be responsible for the timing and magnitude of the $\delta^{13}C$ excursions in these two intervals, and likely in others intervals as well.

The second option, that variations in $\delta^{13}C$ directly reflect variations in the strength and timing of the physical forcings that drive them, is unlikely as well. None of the physical drivers (regional and global tectonics, local and global sea-level changes, or volcanic degassing) are postulated to have declined in the amplitude of their variations on the 0.5–10 M.yr. timescale over the Phanerozoic (Worsley and others, 1984; Haq and others, 1987; Haq and Schutter, 2008; McKenzie and others, 2016).

The interpretation of recurrent $\delta^{13}C$ excursions as a reflection of the action of an oscillatory or repeated forcing that is variably coupled and amplified through a resonant carbon cycle response is largely consistent with geologic constraints. First, a resonant frequency response for the carbon cycle is more likely than a sigmoidal-shaped frequency response, because if the response were sigmoidal, any forcing would have to have a larger amplitude of variation in the 0.5 to 10 M.yr. range than in higher or lower periods in order to account for the increased amplitude of $\delta^{13}C$ variation in that frequency band. Yet, few geological forcings are thought to be characterized by such a frequency distribution. The record of continental flooding (Haq and others, 1987; Haq and Schutter, 2008) suggests that the longer period components (first order changes on the scale of 100 M.yr.) are much larger than the shorter period components (second and third order changes with periods of 0.5–10 M.yr.). The spectral power distributions of the other main possible drivers, tectonics and volcanism, are not known to the same level of detail, but over the Phanerozoic these drivers generally follow the same trends as continental flooding due to the physical connections between them (Worsley and others, 1984; McKenzie and others, 2016). Second, the variable-coupling scenario is more likely than the direct forcing scenario. For most of the fluxes considered in the model, it is unreasonable to assume they act independently of the reservoirs. For example, direct sinusoidal modulation of the phosphate burial flux (F_{bp}) can result in $\delta^{13}C$ excursions with the right durations, but requires that the flux vary independently of phosphate concentrations in the ocean. Furthermore, if directly forced, the forcings on the 0.5 to 10 M.yr. timescale would have had to have diminished in amplitude over the Phanerozoic in order to account for the decline in the amplitude of $\delta^{13}C$ excursions. This is not likely to have been the case.

Due to these considerations, directly forced fluxes or those with sigmoidal frequency responses are unlikely to be able to explain the key features of the carbon isotope record (characteristic duration, declining amplitude), though they surely contributed to the overall shape of the $\delta^{13}C$ frequency distribution (fig. 3). These fluxes include volcanic input (F_v), the weathering of silicates (F_{ws}), the weathering of phosphate (F_{wp}), the burial of phosphate (F_{bp}), and the burial of organic carbon (F_{borg}). The remaining model parameters are the sensitivity of phosphate weathering (k_{wp}), the sensitivity of phosphate burial (k_{bp}), and the sensitivity of organic carbon burial (k_{borg}). These three parameters can be readily mapped to physical scenarios. The former (k_{wp}) represents time-varying changes in weatherability of phosphate, that is, fluctuating phosphate weathering flux at a constant pCO_2 level. In this case the sinusoidal driver can be identified with tectonics (Kump and Arthur, 1997; Caves and others, 2016). The other two parameters map well to a scenario in which sea-level oscillations provide the oscillatory forcing, and anoxia determines the degree to which those oscillations are manifested as time-varying changes in the dependence of the fluxes on the reservoirs. This mapping occurs because anoxia has a strong influence on C:P burial ratio of sediments (Algeo and Ingall, 2007). Directional changes that may account for a decline in coupling between sea-level and tectonics and the fluxes of organic carbon and phosphate have occurred in both the terrestrial and marine realms over the Phanerozoic. Nonetheless, the latter (marine) scenario fits particularly well with geologic evidence. We propose that k_{bp} and k_{borg} have been forced (pseudo) sinusoidally by changes in sea-level, and that the amplitude of this forcing is positively related to the depth and extent of the oxygen minimum zones (OMZs). A model based on similar logic was presented by Lau and others (2016) with the aim of explaining the $\delta^{13}C$ record of a limited interval (the Early to Middle Triassic). Here we expand this model to account for the behavior of the $\delta^{13}C$ record across the Phanerozoic.

During times when the oxygen minimum zones (OMZs) were large and shallow, recurrent sea-level changes would have readily led to large changes in the areal extent

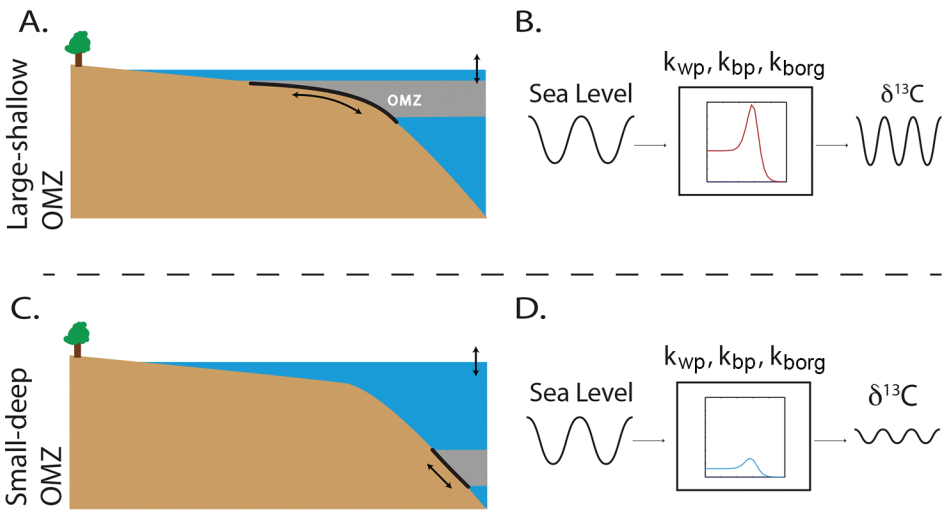

Fig. 12. Proposed linkages between anoxia, sea level, carbon cycle sensitivity, and carbon isotope excursions. (A) When oxygen minimum zones (OMZs) were large, shallow, and prone to expansion, sea-level changes would have had the capacity to drive large changes in the areal extent of OMZs, strongly modulating the C:P burial ratio of organic matter in sediments, and thus global $\delta^{13}C$. (B) Model framework and its relation to the physical scenario. The forcing supplied by sea-level changes would have spanned a range of periods. The model suggests that it is possible that the carbon cycle preferentially amplifies forcings with periods of 0.5–10 M.yr. Thus, changes in sea level need not have had their maximal amplitude of variation in that range, but rather internal carbon cycle amplification can account for the characteristic duration of Phanerozoic carbon isotope excursions. (C) Times in which OMZs were small, deep, and stable, sea-level changes and other forcings would have had much smaller effects on the size of the area in which organic carbon is buried rapidly and efficiently. (D) A decline the extent and depth of ocean anoxia over time resulted in a lowering of the sensitivity of the carbon cycle to physical forcings, and a progressive stabilization of the $\delta^{13}C$ record. Figure modified from Lau and others (2016).

of the anoxic bottom waters, resulting in large variations in the burial sensitivity of carbon and phosphate via changing C:P burial ratios. These changes would have translated into large-amplitude $\delta^{13}C$ excursions (figs. 12A and 12B). In contrast, at times when anoxia was limited to deeper waters, sinusoidal variations in sea level would have led to only slightly modulated burial fluxes resulting in little variation in $\delta^{13}C$ (figs. 12C and 12D). The characteristic period of the resulting $\delta^{13}C$ oscillations can be accounted for by an enhanced sensitivity of the carbon cycle to forcings at those time scales, so that the amplitude of the sea-level variations needn't be largest on the 0.5 to 10 M.yr. periods. The decrease in the amplitude of carbon isotope excursions across the Phanerozoic can be accounted for by an increase in the depth of the OMZs and a decline in the extent of anoxia over that time period.

This model offers an explanation for the common association between positive $\delta^{13}C$ excursions and sea-level highstands (see for example, Cramer and Saltzman, 2007). The correspondence occurs because the highstand is the point at which sea-level is highest and the extent of shelf-depth depositional environments is greatest, so that anoxia reaches its greatest extent resulting in the greatest organic carbon burial. Organic carbon oxidation and negative excursions are expected to be more strongly associated with regressions (with some notable exceptions discussed further below). Maximal organic carbon concentrations (though not necessarily overall burial) are expected to be associated with transgressive sequence tracts. An implication of this association, is that source rock horizons (targets for exploration) should be located at the bases of positive excursions rather than at their apices.

Our proposed mechanism is consistent with the observed decline in baseline levels of anoxia from the Paleozoic to the Mesozoic and Cenozoic. The Paleozoic record is characterized by an unusually large fraction of non-fossiliferous sediments and black shales in sedimentary successions of this age, suggestive of widespread shallow-marine anoxia (Dunbar and Rodgers, 1957; Berry and Wilde, 1978; Peters, 2007). Long-term variation in the magnitude of $\delta^{13}C$ excursions is associated with secular trends in Paleozoic climate and continental flooding. Lower sea level and cooler temperatures in the Late Paleozoic icehouse are associated with few, if any, excursions (fig. 1). While both shallow-marine anoxia and coupling between sea level and organic carbon burial were relatively permanent features of the Paleozoic, during the Mesozoic unusual volcanic outpourings of carbon dioxide were apparently required to raise anoxia onto the shelves and increase the volatility of the $\delta^{13}C$ record (Wignall, 2001; Ganino and Arndt, 2009). Volcanic emanations of carbon likely drove repeated $\delta^{13}C$ excursions by strengthening the coupling of the carbon cycle to sea level via expansion of anoxia rather than by an oscillatory impulsive response of the carbon cycle. A role for anoxia and sea-level changes in driving mass extinctions and delaying the recovery from them has long been recognized (Hallam and Wignall, 1999). Under the proposed mechanism, both the transient coupling of $\delta^{13}C$ to sea level, and the lag between the volcanic perturbation and the most positive $\delta^{13}C$ values following the end-Permian and end-Triassic mass extinctions can readily be explained. Extensive volcanic eruptions triggered expansion of anoxia onto shallow shelf environments, increasing the sensitivity of the carbon cycle to sea level. Once coupled, $\delta^{13}C$ values followed sea level, which need not have reached its maximal value immediately following the volcanic perturbation. Repeated $\delta^{13}C$ oscillations continued until anoxia diminished to pre-perturbations levels, and the coupling to sea level declined in strength.

Volcanic perturbations throughout the Mesozoic and Cenozoic have resulted in progressively smaller $\delta^{13}C$ excursions and more rapid recoveries. The recovery from the end-Permian extinction shows the largest $\delta^{13}C$ excursions (fig. 1C). The end-Triassic extinction was followed by excursions smaller than those that follow the end-Permian extinction, but still bigger than those associated with later OAEs (fig. 1D). The PETM and other Cenozoic hyperthermals exhibit still smaller carbon isotope excursions than Mesozoic OAEs and earlier mass extinction events. The Cenozoic excursions are quite muted in comparison to those of the Paleozoic and Mesozoic, and similar to the highly damped model responses to an impulsive perturbation (fig. 8A). A progressive deepening of the OMZ and a reduction in its size, likely modulated by such factors as temperature and its impacts on respiration (Finnegan and others, 2012), and the strength of the biological pump (Logan and others, 1995; Meyer and others, 2016), would be expected to result in a diminishing link between the carbon cycle and sea level, and a reduced sensitivity to physical disturbances resulting in an increasingly stable $\delta^{13}C$ record.

A monotonic increase in atmospheric pO_2 over the Phanerozoic is not required to explain the decline in the amplitude of $\delta^{13}C$ excursions. Rather than atmospheric O_2 being the primary control on the extent of ocean anoxia, we envision changing ocean redox conditions as likely to have been primarily controlled by biology. The redox conditions at any point within the ocean reflect the balance between the rate of organic carbon degradation (and oxygen consumption) on the one hand, and the rate at which oxidants are supplied to the site of organic carbon degradation via advection and diffusion on the other. Biology has likely influenced both sides of the balance. Increasing depth of bioturbation across the Phanerozoic (Droser and Bottjer, 1993) would have led to improved ventilation of sediments, increasing the efficacy of organic carbon degradation and leading to a reduction in the positive feedbacks that underpin the anoxia-productivity feedback. Increasing availability of well-oxygenated habitats for bioturbating fauna would have promoted their diversification, feeding back onto

suppression of anoxia. Appearance of pelagic calcifiers and increased ballasting of organic carbon from the mid-Mesozoic onwards would have further accelerated the stabilization trends (Ridgwell and Zeebe, 2005) by increasing the speed at which organic particles travel through the water column.

Not that atmospheric O_2 levels did not matter for Phanerozoic carbon cycle dynamics. It is likely, however, that short-term excursions in pO_2 were more important than previously estimated, and long-term trends overstated. The more highly resolved $\delta^{13}C$ data indicate that the mid-Paleozoic peak in the long-term $\delta^{13}C$ trend (fig. 2A) is far less ^{13}C-enriched than the inputs used for modeling pO_2 in previous modeling efforts (Berner, 2001), suggesting less variation in pO_2 on those timescales than previously envisioned, and likely much more variation on the 0.5 to 10 M.yr. timescale. These rapid changes in pO_2 (Saltzman and others, 2011) would have potentially provided an additional contribution to the sinusoidal modulation of the burial fluxes of organic carbon and phosphate beyond what is outlined by the current model.

The hypsometry of the shelves and extent of continental flooding likely also played a role in modulating the $\delta^{13}C$ response to sea-level oscillations over the Phanerozoic. A lower extent of continental flooding would have forced OMZs to sit lower on the slope, hence making their areal extent harder to force with smaller-order changes in base level regardless of oxygenation. The changes in envelope of third-order $\delta^{13}C$ variations over the Phanerozoic occur on a similar timescale (~50 M.yr.), and correspond sufficiently well to Phanerozoic sedimentary sequences (Sloss, 1963), to suggest that secular variations in the extent of continental flooding may have exerted a control on their timing.

The sea-level changes considered here need not have been strictly eustatic, but rather only sufficiently widespread so that they effected significant leverage on the globally integrated burial flux of organic carbon. Neither must the output of ^{13}C-depleted carbon have been exclusively via organic carbon burial. Authigenic carbonate produced during early diagenesis (Schrag and others, 2013) may have also increased during anoxic events (Greene and others, 2012) amplifying $\delta^{13}C$ changes beyond our model estimates. The proportions of the two fluxes may have also shifted over the course of Earth's history as a function of the availability of oxidants (for example, sulfate and nitrate), and the strength of the biological pump (Higgins and others, 2009). It is possible that at times the weathering and burial of authigenic carbon were the more dominant fluxes. If so, our proposed model still holds, although the $\delta^{13}C$ values of shallow marine carbonates then reflect a more indirect impact of sea-level and redox conditions. Nonetheless, such secular variations (if they indeed occurred) should be easy to incorporate into our proposed framework. Variations in the isotopic composition of carbon inputs would have been another potential source of variability impacting the $\delta^{13}C$ record. During regressions, the carbon isotopic composition of the weathering input will depend on the proportions of carbonate and organic carbon being eroded, and their respective isotopic compositions (Gibbs and others, 1999). Regression leading to exposure of abundant ^{13}C-enriched carbonates with little organic matter oxidation might result in a shift to more ^{13}C-enriched values (Kump and Arthur, 1999). The relative proportions of carbonate weathering and organic carbon oxidation were likely impacted by changes in atmospheric O_2 over Earth's history (Holland, 1984), in addition to having a tectonic control.

Extension to the Proterozoic

The interplay between hypsometry of the continental shelves and the structure of ocean redox conditions may explain certain aspects of the Proterozoic carbon isotope record as well. Maximal sensitivity of the extent of anoxia on sea-level variations would be achieved when anoxic bottom waters are overlain by oxygenated surface waters, and the contact between the two is situated near the shelf-slope break. In such a case, small

sea level changes would suffice to drive large increases in the areal extent of anoxic waters. Conversely, in a world in which the entire water column is anoxic, small sea-level changes would not affect burial fluxes of organic carbon and phosphate as much. Nonetheless, large sea-level changes could potentially result in dramatic changes in $\delta^{13}C$ as complete exposure of the shelves would result in the oxidation of all the organic carbon previously deposited on them. The effect would be maximized when the surface ocean is sufficiently oxygenated such that during regressions organic matter being weathered off the exposed shelves would enter into oxygenated waters resulting in rapid oxidation (Goldblatt and others, 2006).

The prevailing paradigm is that the Mesoproterozoic was less well oxygenated than the Neoproterozoic, and the Neoproterozoic was less oxygenated still than the Phanerozoic (Lyons and others, 2014). Thus, the transition from the $\delta^{13}C$ stability of the Mesoproterozoic to the turmoil of the Neoproterozoic and the increasing stability of the Phanerozoic could reflect an increase in the oxygenation state of the ocean. In particular, a combination of very shallow OMZs (relative to the shelf break) and sufficiently oxygenated surface waters may explain why the Neoproterozoic $\delta^{13}C$ oscillations have much larger amplitudes and periods than the Phanerozoic ones. The modeling indicates that Neoproterozoic-style oscillations can occur without violation of mass balance (that is negative mass), suggesting that such large and protracted excursions could arise with sufficient forcing by sea-level.

Changes in global hypsometry and continental area may have also played a role. The Neoproterozoic was a period of protracted continental emergence (Peters and Gaines, 2012) associated with a dramatic increase in sediment storage capacity (Husson and Peters, 2017). These lines of evidence suggest a period of continental growth followed by a major increase in the area of continental flooding. If so, growth of shallow continental shelves during the Neoproterozoic could have led to a strong coupling between sea level and redox conditions, resulting in strong modulation of the carbon cycle and large $\delta^{13}C$ oscillations. It is also possible that the associated increase in terrestrially derived phosphate (Reinhard and others, 2016) played a role by increasing nutrient loadings. Low rates of arc volcanism would have set the boundary conditions for Cryogenian glaciations (McKenzie and others, 2016). Abundant anaerobic degradation of organic carbon and associated alkalinity production would have led to some regressions triggering Snowball Earth conditions (Tziperman and others, 2011). This period of instability persisted until base levels of O_2 in the atmosphere increased sufficiently to induce more extensive aerobic oxidation of organic carbon and amelioration of the anoxia-productivity feedbacks, thus setting the stage for Phanerozoic $\delta^{13}C$ stabilization.

CONCLUSIONS

Decreased anoxia in shallow marine environments may explain more than just the decreased volatility of the carbon isotopic record across the Phanerozoic. The implied decrease in the frequency and extent of shallow-marine anoxia can also help to account for declining background extinction intensity across the Phanerozoic (Raup and Sepkoski, 1982), as well as directional trends from smaller, sessile and less active organisms, to larger, more mobile and more predatory organisms (Bush and Bambach, 2011; Heim and others, 2015). We speculate that the trends in both the biotic and $\delta^{13}C$ records result from the progressive oxygenation of the oceans, which caused a decline in the extent and severity of anoxia, a decrease in the frequency of incursions of anoxic waters onto the shelves, and the migration of the OMZs from the shallow shelves, where most organisms reside, to the deeper ocean. The linked biotic and geochemical feedbacks resulted in the progressive stabilization of the Earth System.

Author contributions:

AB and LRK conceived the study; AB, KVL, and JLP developed the ideas; AB carried out the analyses and wrote the bulk of the paper. All authors contributed to data interpretation and commented extensively on the paper. The authors declare no conflict of interests.

ACKNOWLEDGMENTS

The authors thank Jon Husson, Chris Reinhard, and an anonymous reviewer for comments that greatly improved the manuscript. Reinhard is particularly thanked for proposing the term "harmonic" for this view of the $\delta^{13}C$ record. AB would further like to thank Paul Hoffman for providing him with an opportunity to view the Snowball Earth successions in Namibia, and for long nights around the campfire in which some of the ideas presented in this work were catalyzed.

APPENDIX

CONDITION FOR OSCILLATIONS

Derivation

The relationship between the coefficients and the behavior of the system can be formally established. (See the Appendix [1], for a similar development in a climate modeling context. See [2], and [3, 4], for related mathematical treatments in a geochemical context. See [5], for an approachable introduction to linear systems from a control theory standpoint and [6], for an introduction with a mechanical and electrical engineering flavor.)

The matrix form of the system is given by:

$$\begin{bmatrix} \dot{M}_P \\ \dot{M}_C \end{bmatrix} = \begin{bmatrix} -k_{bp} & k_{wp} \\ -k_{bo} & -k_{ws} \end{bmatrix} \begin{bmatrix} M_P \\ M_C \end{bmatrix} + \begin{bmatrix} 0 \\ F_v + F_{wo} \end{bmatrix}$$

Or more compactly:

$$\dot{\vec{M}} = K\vec{M} + \vec{F}$$

The behavior of the system is determined by the eigenvalues of the coefficient matrix:

$$K = \begin{bmatrix} -k_{bp} & k_{wp} \\ -k_{bo} & -k_{ws} \end{bmatrix}$$

These can be calculated via the eigenvalue equation:

$$K\vec{x} = \lambda\vec{x}$$

A nontrivial solution exists only when the determinant of $\lambda I - K$ equals zero:

$$\begin{vmatrix} \lambda + k_{bp} & -k_{wp} \\ k_{bo} & \lambda + k_{ws} \end{vmatrix} = (\lambda + k_{bp})(\lambda + k_{ws}) + k_{wp}k_{bo} = 0$$

The resulting characteristic polynomial is:

$$\lambda^2 + (k_{bp} + k_{ws})\lambda + k_{bp}k_{ws} + k_{wp}k_{bo}$$

Whose roots are given by:

$$\lambda_{1,2} = \frac{-(k_{bp} + k_{ws}) \pm \sqrt{(k_{bp} + k_{ws})^2 - 4(k_{bp}k_{ws} + k_{wp}k_{bo})}}{2}$$

Oscillatory solutions (complex eigenvalues) exist when the discriminant is less than zero:

$$(k_{bp} + k_{ws})^2 - 4(k_{bp}k_{ws} + k_{wp}k_{bo}) < 0$$

Gathering terms gives the condition for oscillations.

$$(k_{bp} - k_{ws})^2 < 4(k_{wp}k_{bp})$$

Comparison With a Mass-Spring Harmonic Oscillator

In a mass-spring system the forces in operation are the force exerted on the mass by the spring, and the friction operating on the mass. We assume that the force exerted by the spring is linearly related to the displacement of the spring (Hook's law), and the damping is linearly dependent on the velocity of the mass. The sum of the two forces are equal to the change in momentum as expressed by F = ma, or in its differential form:

$$-kx - c\frac{dx}{dt} = m\frac{d^2x}{dx^2}$$

Since there is an equivalency between a large mass on a large spring and a small mass on a small spring, it is convenient to introduce non-dimensional variables, the angular frequency and the damping ratio:

$$\omega_0 = \sqrt{\frac{k}{m}} \quad \zeta = \frac{c}{2\sqrt{mk}}$$

The equation of motion then becomes:

$$\frac{d^2x}{dt^2} + 2\zeta\omega_0\frac{dx}{dt} + \omega_0^2 x = 0$$

This equation can be converted to two first order differential equations by defining x_1, position, and x_2, velocity:

$$\frac{dx_1}{dt} = x_2$$

$$\frac{dx_2}{dt} = -2\zeta\omega_0 x_2 - \omega_0^2 x_1$$

Writing the system in matrix form reveals the similarity to the carbon cycle model.

$$\begin{bmatrix} \dot{x}_1 \\ \dot{x}_2 \end{bmatrix} = \begin{bmatrix} 0 & 1 \\ -\omega_0^2 & -2\zeta\omega_0 \end{bmatrix} \begin{bmatrix} x_1 \\ x_2 \end{bmatrix}$$

Here the "cross" terms are 1 and $-\omega_0^2$. The characteristic polynomial is:

$$\begin{vmatrix} \lambda & -1 \\ \omega_0^2 & \lambda + 2\zeta\omega_0 \end{vmatrix} = \lambda^2 + 2\zeta\omega_0\lambda + \omega_0^2$$

Oscillatory solutions (complex eigenvalues) exist when the discriminant is less than zero:

$$4\omega_0^2(\zeta^2 - 1) < 0$$

Hence, when $\zeta < 1$ the system will be underdamped and oscillate, whereas when $\zeta > 1$ the system will exhibit smoothly decaying solutions.

TABLE A1

Descriptive statistics of Phanerozoic $\delta^{13}C$ Data

Period	Duration [M.yr.]	Number of unique data points	Average data spacing [yr]	Data density [points/M.yr.]
Cenozoic	66.18	27259	4125	242
Cenozoic (downsampled)	66.18	481	135,536	7.4
Cretaceous	80.18	229	350,162	1.6
Jurassic	54.51	238	229,035	4.3
Triassic	50.58	595	85,479	11.76
Permian	46.72	414	113,123	8.8
Carboniferous	60.05	1133	53,000	18.9
Devonian	60.25	900	66,945	14.9
Silurian	24.51	626	39,345	24.5
Ordovician	44.09	673	67,101	14.9
Cambrian	55.63	1984	28,053	35.6
Total	542.7	6564	119845	14.1

TABLE A2

Model Values

Variable Name		Steady State Value [mol] or [mol yr^{-1}]
M_P		$2x10^{15}$
M_C		$3.8x10^{18}$
F_{wp}		$3.6x10^{10}$
F_{bp}		$3.6x10^{10}$
F_v		$4x10^{12}$
F_{ws}		$4x10^{12}$
F_{bo}		$12x10^{12}$
F_{wo}		$12x10^{12}$
Coefficient Name	Calculated via	Steady State Value [yr^{-1}]
k_{wp}	F_{wp}/M_C	$9.4737x10^{-9}$
k_{bp}	F_{bp}/M_P	$1.8x10^{-5}$
k_{bo}	F_{bo}/M_P	$6x10^{-3}$
k_{ws}	F_{ws}/M_C	$1.0562x10^{-6}$

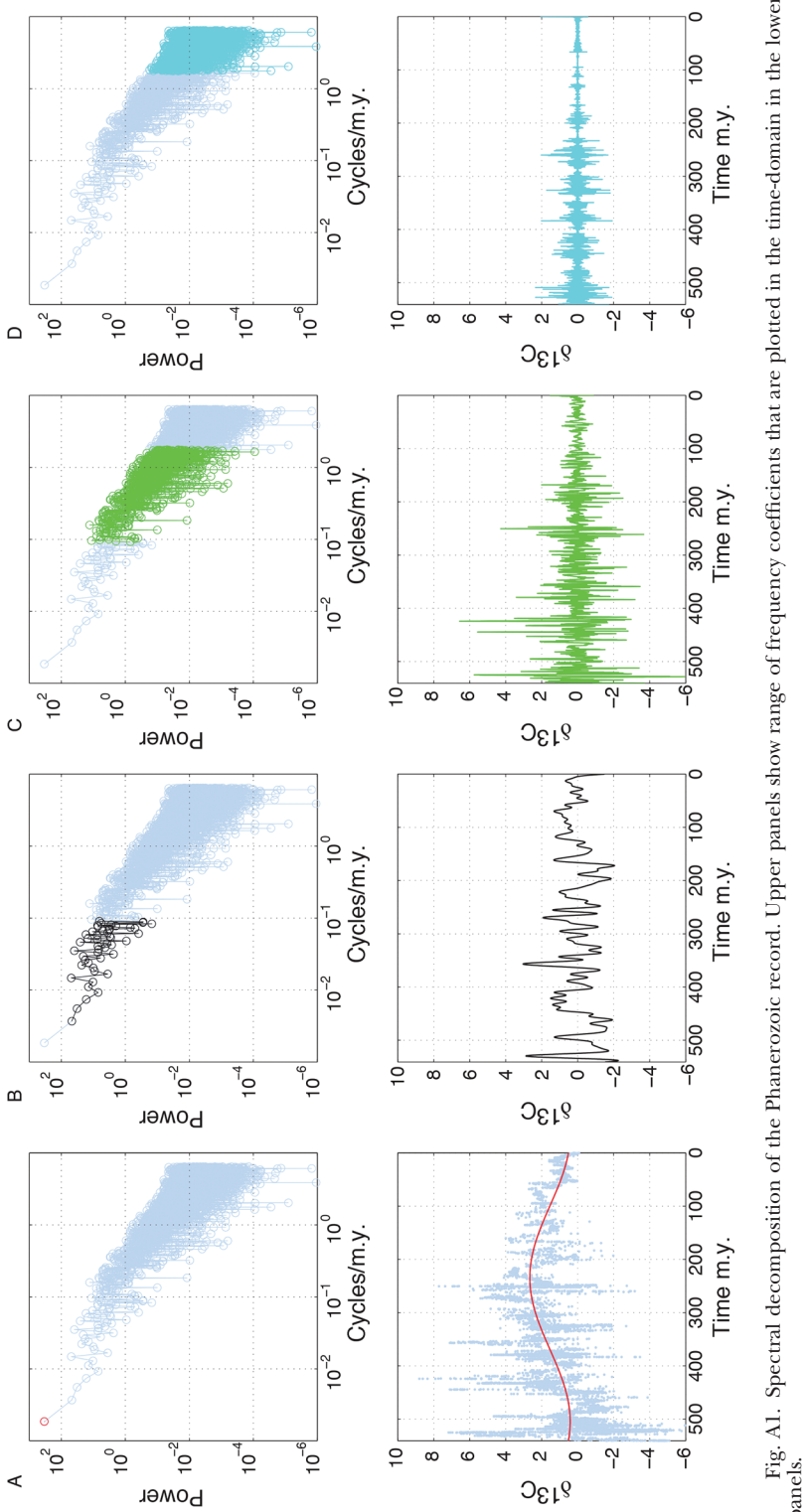

Fig. A1. Spectral decomposition of the Phanerozoic record. Upper panels show range of frequency coefficients that are plotted in the time-domain in the lower panels.

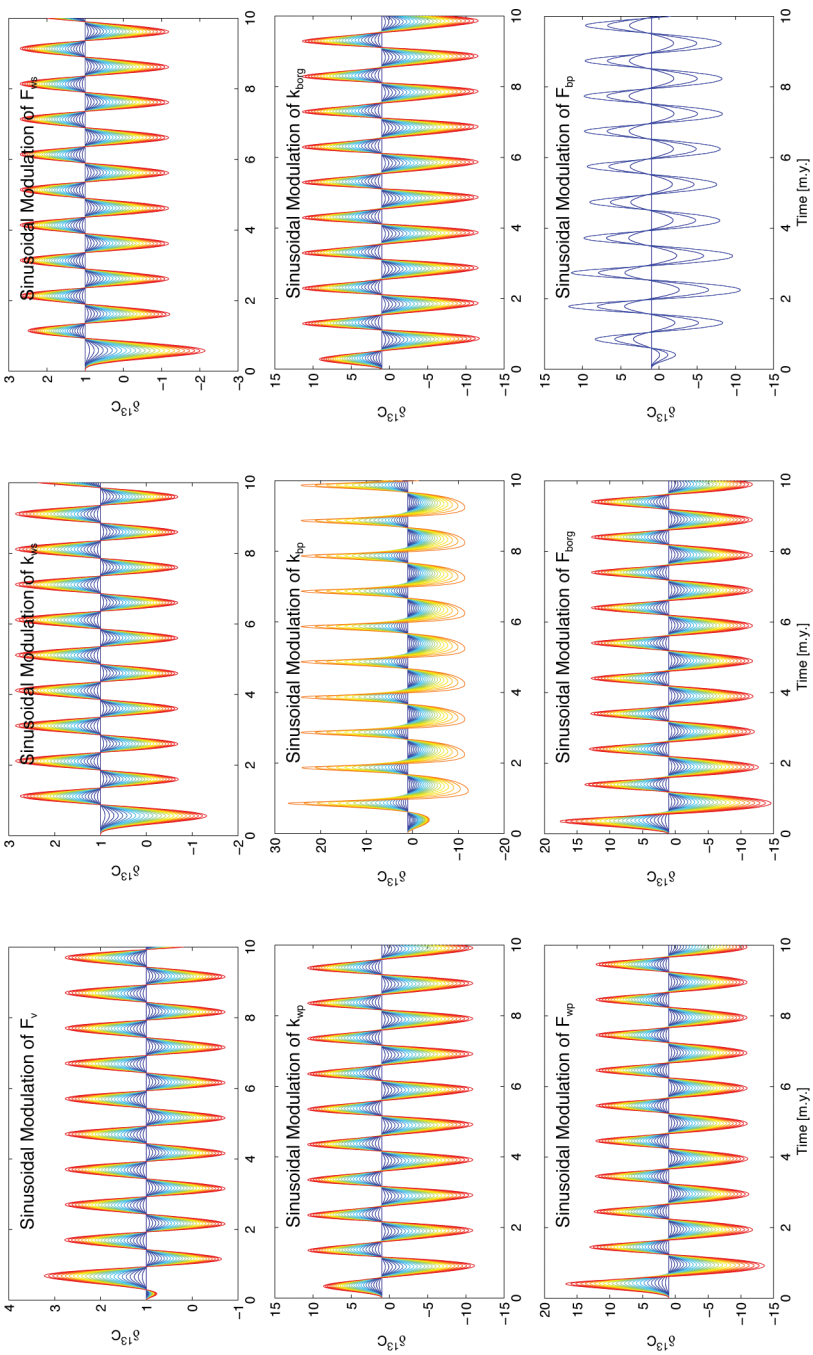

Fig. A2-A. Model $\delta^{13}C$ response to sinusoidal modulation of parameters with a period of 1 m.y. The flux being modulated in each instance is denoted by the name of the flux in the upper part of the subplot (for example F_v). Modulation of a flux coefficient is denoted by the name of the rate parameter (for example k_{wp}). The resulting $\delta^{13}C$ output is given as a function of time. Frequency and amplitude combinations resulting in non-physical reservoir values (negative mass) were not plotted.

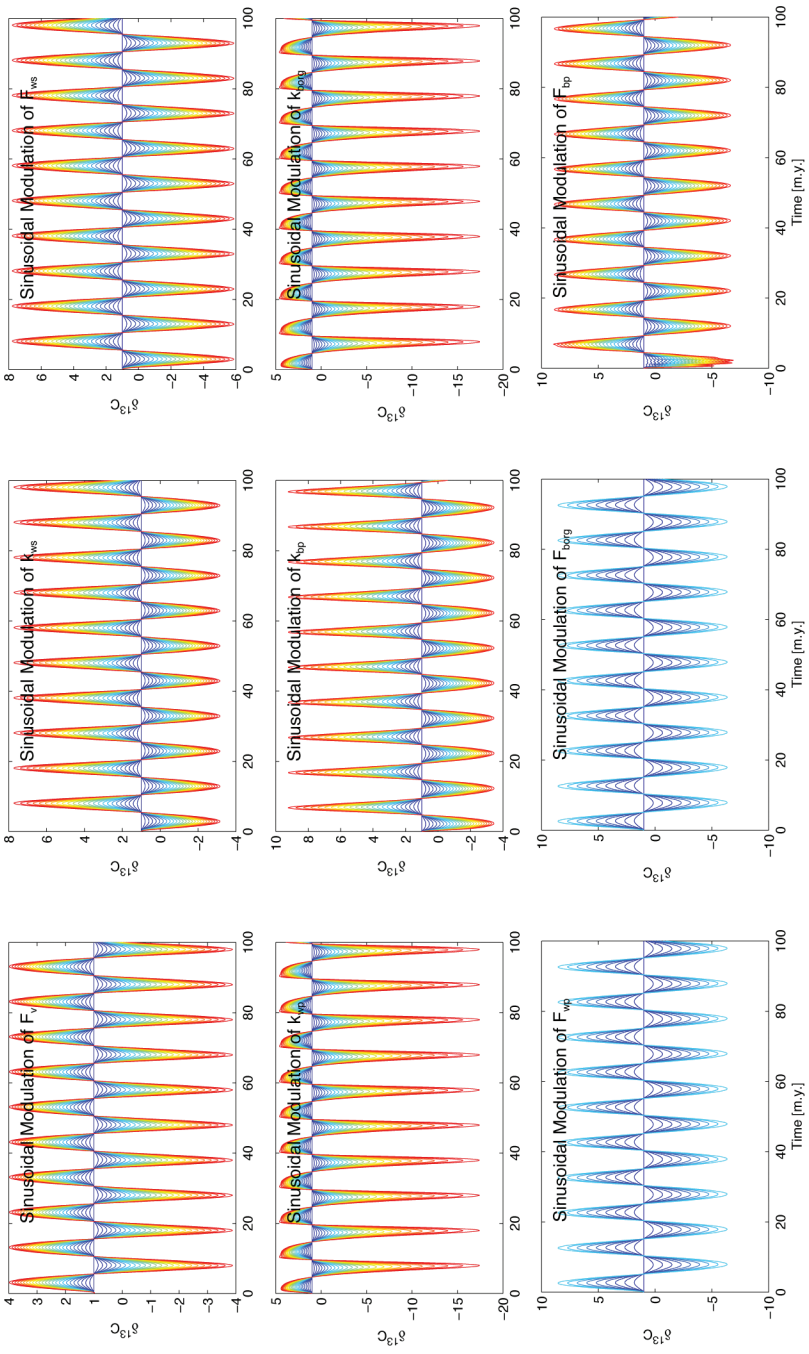

Fig. A2-B. Same as in figure A2-A but with a period of forcing of 10 m.y.

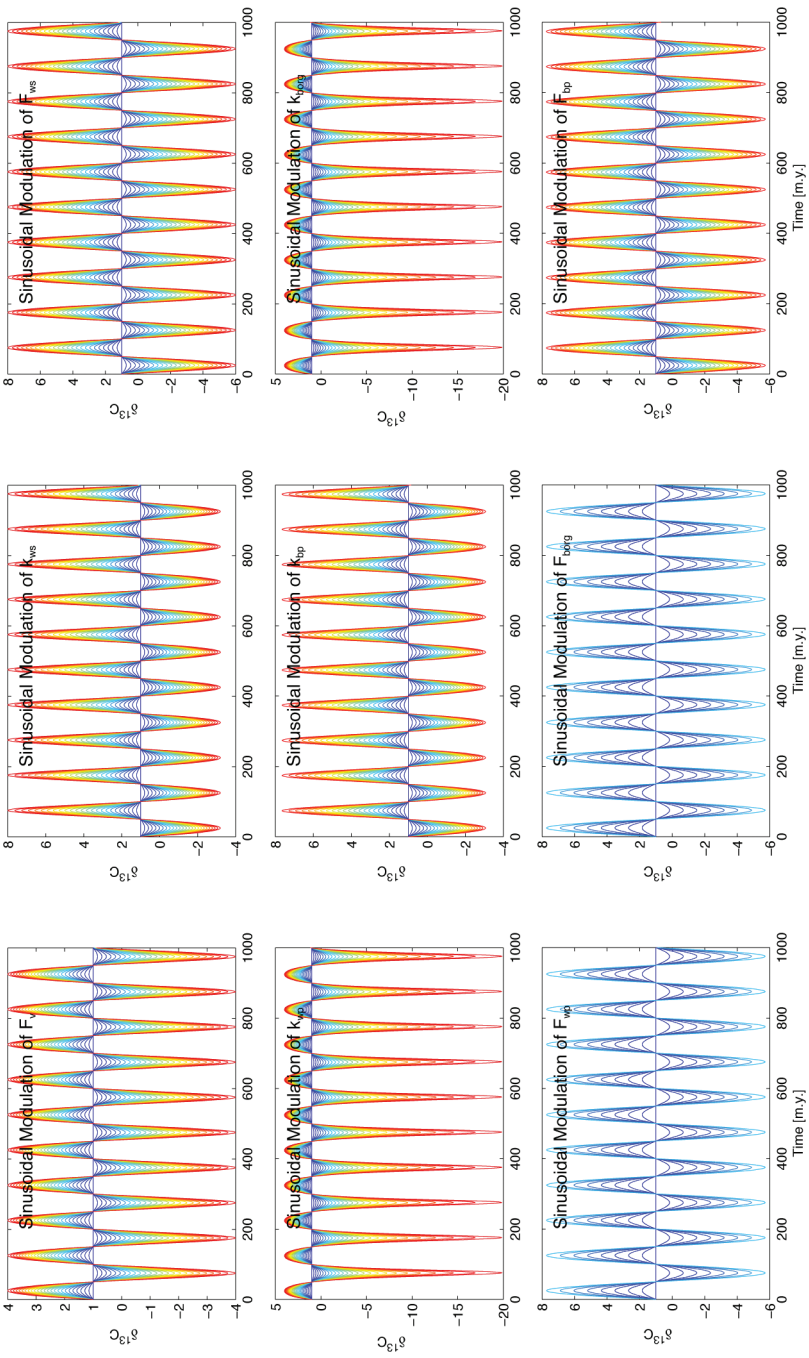

Fig. A2-C. Same as in figure A2-A but with a period of forcing of 100 m.y.

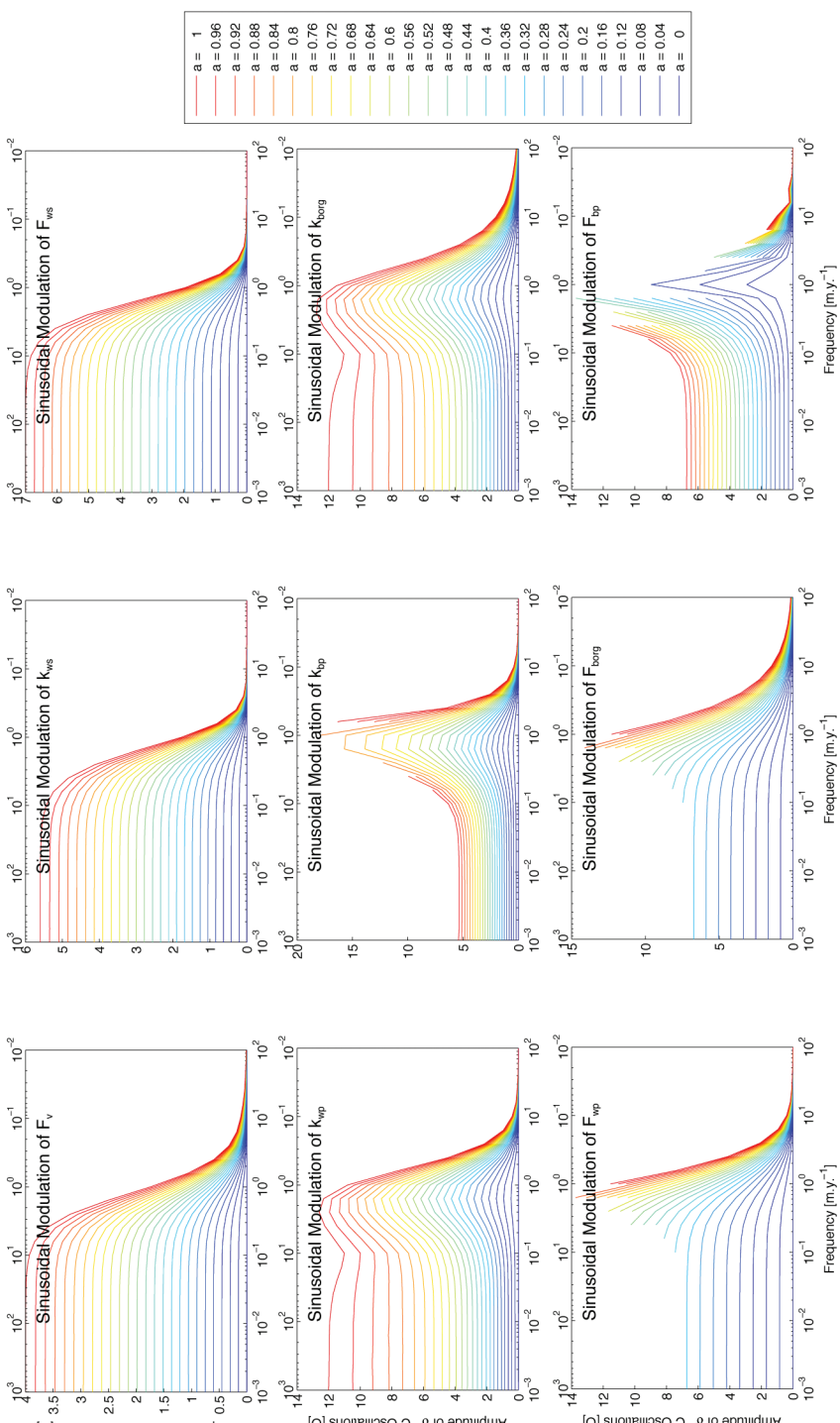

Fig. A3. Model $\delta^{13}C$ response to sinusoidal modulation of parameters. Modulation of a flux is denoted by the name of the flux (for example F_v). Modulation of a flux sensitivity is denoted by the name of the rate parameter (for example k_{wp}). Amplitude of the resulting $\delta^{13}C$ oscillations on the y-axis, frequency on the lower x-axis, and period of forcing on the upper x-axis. Frequency and amplitude combinations resulting in non-physical reservoir values (negative mass) were not plotted, hence the truncation of some lines.

APPENDIX REFERENCES

[1] Pollard, D., Kump, L., and Zachos, J., 2013, Interactions between carbon dioxide, climate, weathering, and the Antarctic ice sheet in the earliest Oligocene: Global and Planetary Change, v. 111, p. 258–267, https://doi.org/10.1016/j.gloplacha.2013.09.012
[2] Southam, J. R., and Hay, W.W., 1976, Dynamical formulation of Broecker's model for marine cycles of biologically incorporated elements: Journal of the International Association for Mathematical Geology, v. 8, n. 5, p. 511–527, https://doi.org/10.1007/BF01042991
[3] Lasaga, A. C., 1980, The kinetic treatment of geochemical cycles: Geochimica et Cosmochimica Acta, v. 44, n. 6, p. 815–828, https://doi.org/10.1016/0016-7037(80)90263-X
[4] Lasaga, A. C., 1981, Dynamic treatment of geochemical cycles: global kinetics, *in* Lasaga, A., and Kirkpatrick, R., editors,: Reviews in Minearology and Geochemistry, v. 8, p. 69–110.
[5] Aström, K., J., and Murray, R. M., 2010, Feedback Systems: An Introduction for Scientists and Engineers: Princeton, New Jersey, Princeton University Press, 408 p.
[6] Lathi, B. P., 1992, Linear systems and signals: Carmichael, California, Berkeley-Cambridge Press, 656 p.

REFERENCES

Algeo, T. J., and Ingall, E., 2007, Sedimentary C_{org}: P ratios, paleocean ventilation, and Phanerozoic atmospheric pO_2: Palaeogeography, Palaeoclimatology, Palaeoecology, v. 256, n. 3–4, p. 130–155, https://doi.org/10.1016/j.palaeo.2007.02.029
Algeo, T. J., and Twitchett, R. J., 2010, Anomalous Early Triassic sediment fluxes due to elevated weathering rates and their biological consequences: Geology, v. 38, n. 11, p. 1023–1026, https://doi.org/10.1130/G31203.1
Arvidson, R. S., Mackenzie, F. T., and Guidry, M., 2006, MAGic: A Phanerozoic model for the geochemical cycling of major rock-forming components: American Journal of Science, v. 306, v. 3, p. 135–190, https://doi.org/10.2475/ajs.306.3.135
Aström, K. J., and Murray, R. M., 2010, Feedback Systems: An Introduction for Scientists and Engineers: Princeton, New Jersey, Princeton University Press, 408 p.
Bachan, A., van de Schootbrugge, B., Fiebig, J., McRoberts, C. A., Ciarapica, G., and Payne, J. L., 2012, Carbon cycle dynamics following the end-Triassic mass extinction: Constraints from paired $\delta^{13}C_{carb}$ and $\delta^{13}C_{org}$ records: Geochemistry, Geophysics, Geosystems, v. 13, n. 9, p. Q09008, https://doi.org/10.1029/2012GC004150
Bergman, N. M., Lenton, T. M., and Watson, A. J., 2004, COPSE: A new model of biogeochemical cycling over Phanerozoic time: American Journal of Science, v. 304, n. 5, p. 397–437, https://doi.org/10.2475/ajs.304.5.397
Berner, R. A., 1987, Models for carbon and sulfur cycles and atmospheric oxygen: Application to Paleozoic geologic history: American Journal of Science, p. 287, n. 3, p. 177–196, https://doi.org/10.2475/ajs.287.3.177
——— 1991, A model for atmospheric CO_2 over Phanerozoic time: American Journal of Science, v. 291, n. 4. p. 339–376, https://doi.org/10.2475/ajs.291.4.339
——— 1994, Geocarb II: A revised model of atmospheric CO_2 over Phanerozoic time: American Journal of Science, v. 294, n. 1, p. 56–91, https://doi.org/10.2475/ajs.294.1.56
——— 2001, Modeling atmospheric O_2 over Phanerozoic time: Geochimica et Cosmochimica Acta, v. 65, n. 5, p. 685–694, https://doi.org/10.1016/S0016-7037(00)00572-X
——— 2006, GEOCARBSULF: A combined model for Phanerozoic atmospheric O_2 and CO_2: Geochimica et Cosmochimica Acta, v. 70, n. 23, p. 5653–5664, doi:10.1016/j.gca.2005.11.032
Berner, R. A., and Canfield, D. E., 1989, A new model for atmospheric oxygen over Phanerozoic time: American Journal of Science, v. 289, n. 4, p. 333–361, https://doi.org/10.2475/ajs.289.4.333
Berner, R. A., and Kothavala, Z., 2001, Geocarb III: A revised model of atmospheric CO_2 over Phanerozoic time: American Journal of Science, v. 301, n. 2, p. 182–204, https://doi.org/10.2475/ajs.301.2.182
Berner, R. A., Lasaga, A. C., and Garrels, R. M., 1983, The carbonate-silicate geochemical cycle and its effect on atmospheric carbon dioxide over the past 100 million years: American Journal of Science, v. 283, n. 7, p. 641–683, https://doi.org/10.2475/ajs.283.7.641
Berry, W. B. N., and Wilde, P., 1978, Progressive ventilation of the oceans—An explanation for the distribution of the lower Paleozoic black shales: American Journal of Science, v. 278, n. 3, p. 257–275, https://doi.org/10.2475/ajs.278.3.257
Bjerrum, C. J., and Canfield, D. E., 2004, New insights into the burial history of organic carbon on the early earth: Geochemistry, Geophysics, Geosystems, v. 5, n. 8, p. Q08001, https://doi.org/10.1029/2004GC000713
Blackburn, T. J., Olsen, P. E., Bowring, S. A., McLean, N. M., Kent, D. V., Puffer, J., McHone, G., Rasbury, E. T., and Et-Touhami, M., 2013, Zircon U-Pb Geochronology Links the End-Triassic Extinction with the Central Atlantic Magmatic Province: Science, v. 340, n. 6135, p. 941–945, https://doi.org/10.1126/science.1234204
Bolton, E. W., Berner, R. A., and Petsch, S. T., 2006, The weathering of sedimentary organic matter as a control on atmospheric O_2: II. Theoretical modeling: American Journal of Science, v. 306, n. 8, p. 575–615, https://doi.org/10.2475/08.2006.01
Boss, S. K., and Wilkinson, B. H., 1991, Planktogenic/eustatic control on cratonic/oceanic carbonate accumulation: The Journal of Geology, v. 99, n. 4, p. 497–513, https://doi.org/10.1086/629513

Broecker, W. S., 1971, A kinetic model for the chemical composition of sea water: Quaternary Research, v. 1, n. 2, p. 188–207, https://doi.org/10.1016/0033-5894(71)90041-X
Burgess, S. D., and Bowring, S. A., 2015, High-precision geochronology confirms voluminous magmatism before, during, and after Earth's most severe extinction: Science Advances, v. 1, n. 7, https://doi.org/10.1126/sciadv.1500470
Bush, A. M., and Bambach, R. K., 2011, Paleoecologic Megatrends in Marine Metazoa: Annual Review of Earth and Planetary Sciences, v. 39, n. 1, p. 241–269, https://doi.org/10.1146/annurev-earth-040809-152556
Caves, J. K., Jost, A. B., Lau, K. V., and Maher, K., 2016, Cenozoic carbon cycle imbalances and a variable weathering feedback: Earth and Planetary Science Letters, v. 450, p. 152–163, https://doi.org/10.1016/j.epsl.2016.06.035
Chang, S., and Berner, R. A., 1999, Coal weathering and the geochemical carbon cycle: Geochimica et Cosmochimica Acta, v. 63, n. 19, p. 3301–3310, https://doi.org/10.1016/S0016-7037(99)00252-5
Clarke, F., 1924, The data of geochemistry: US Geological Survey Bulletin, v. 770, p. 841.
Craig, H., 1953, The geochemistry of the stable carbon isotopes: Geochimica et Cosmochimica Acta, v. 3, n. 2–3, p. 53–92, https://doi.org/10.1016/0016-7037(53)90001-5
Cramer, B. D., and Saltzman, M. R., 2007, Fluctuations in epeiric sea carbonate production during Silurian positive carbon isotope excursions: A review of proposed paleoceanographic models: Palaeogeography, Palaeoclimatology, Palaeoecology, v. 245, n. 1–2, p. 37–45, https://doi.org/10.1016/j.palaeo.2006.02.027
Cui, H., Kaufman, A. J., Xiao, S., Zhou, C., and Liu, X-M., 2017, Was the Ediacaran Shuram excursion a globally synchronized early diagenetic event? Insights from methane-derived authigenic carbonates in the uppermost Doushantuo Formation, South China: Chemical Geology, v, 450, p. 59–80, https://doi.org/10.1016/j.chemgeo.2016.12.010
Dunbar, C. O., and Rodgers, J., 1957, Principles of stratigraphy: New York, John Wiley, 356 p.
Droser, M. L., and Bottjer, D. J., 1993, Trends and Patterns of Phanerozoic Ichnofabrics: Annual Review of Earth and Planetary Sciences, v. 21, n. 1, p. 205–225, https://doi.org/10.1146/annurev.ea.21.050193.001225
Erba, E., Channell, J. E. T., Claps, M., Jones, C., Larson, R., Opdyke, B., Silva, I. P., Riva, A., Salvini, G., and Torricelli, S., 1999, Integrated stratigraphy of the Cismon Apticore (southern Alps, Italy): A "reference section" for the Barremian-Aptian interval at low latitudes: Journal of Foraminiferal Research, v. 29, n. 4, p. 371–391.
Finnegan, S., Fike, D. A., Jones, D., and Fischer, W. W., 2012, A Temperature-Dependent Positive Feedback on the Magnitude of Carbon Isotope Excursions: Geoscience Canada, v. 39, n. 3, p. 122–131.
Froelich, P. N., Bender, M. L., Luedtke, N. A., Heath, G. R., and DeVries, T., 1982, The marine phosphorus cycle: American Journal of Science, v. 282, n. 4, p. 474–511, https://doi.org/10.2475/ajs.282.4.474
Gale, A. S., Jenkyns, H. C., Kennedy, W. J., and Corfield, R. M., 1993, Chemostratigraphy versus biostratigraphy: data from around the Cenomanian–Turonian boundary: Journal of the Geological Society, v. 150, n. 1, p. 29–32, https://doi.org/10.1144/gsjgs.150.1.0029
Ganino, C., and Arndt, N. T., 2009, Climate changes caused by degassing of sediments during the emplacement of large igneous provinces: Geology, v. 37, n. 4, p. 323–326, https://doi.org/10.1130/G25325A.1
Garrels, R. M., and Lerman, A., 1984, Coupling of the sedimentary sulfur and carbon cycles; an improved model: American Journal of Science, v. 284, n. 9, p. 989–1007, https://doi.org/10.2475/ajs.284.9.989
Garrels, R. M., and Perry, E. A., Jr., 1974, Cycling of carbon, sulphur and oxygen through geologic time, *in* Goldberg, E., editor, The sea: Ideas and Observations on Progress in the Study of the Seas, v. 5: New York, J. Wiley, p. 303–336.
Gibbs, M. T., Bluth, G. J., Fawcett, P. J., and Kump, L. R., 1999, Global chemical erosion over the last 250 My: Variations due to changes in paleogeography, paleoclimate, and paleogeology: American Journal of Science, v. 299, n. 7–9, p. 611–651, https://doi.org/10.2475/ajs.299.7-9.611
Gischler, E., Swart, P. K., and Lomanodo, A. J., 2009, Stable isotopes of carbon and oxygen in modern sediments of carbonate platforms, barrier reefs, atolls and ramps: Patterns and implications, *in* Swart, P. K., Eberli, G. P., McKenzie, J. A., Jarvis, I., and Stevens, T., editors, Perspectives in Carbonate Geology: A Tribute to the Career of Robert Nathan Ginsburg: International Association of Sedimentologists Special Publication, v. 41, p. 61–74, https://doi.org/10.1002/9781444312065.ch5
Goldblatt, C., Lenton, T. M., and Watson, A. J., 2006, Bistability of atmospheric oxygen and the Great Oxidation: Nature, v. 443, n. 7112, p. 683–686, https://doi.org/10.1038/nature05169
Greene, S. E., Bottjer, D. J., Corsetti, F. A., Berelson, W. M., and Zonneveld, J-P., 2012, A subseafloor carbonate factory across the Triassic-Jurassic transition: Geology, v. 40, n. 11, p. 1043–1046, https://doi.org/10.1130/G33205.1
Grötsch, J., Billing, I., and Vahrenkamp, V., 1998, Carbon-isotope stratigraphy in shallow-water carbonates: Implications for Cretaceous black-shale deposition: Sedimentology, v. 45, n. 4, p. 623–634, https://doi.org/10.1046/j.1365-3091.1998.00158.x
Hallam, A., and Wignall, P. B., 1999, Mass extinctions and sea-level changes: Earth-Science Reviews, v. 48, n. 4, p. 217–250, https://doi.org/10.1016/S0012-8252(99)00055-0
Halverson, G. P., Hoffman, P. F., Schrag, D. P., Maloof, A. C., and Rice, A. H. N., 2005, Toward a Neoproterozoic composite carbon-isotope record: Geological Society of America Bulletin, v. 117, n. 9–10, p. 1181–1207, https://doi.org/10.1130/B25630.1
Hannisdal, B., and Peters, S. E., 2011, Phanerozoic Earth System Evolution and Marine Biodiversity: Science, v. 334, n. 6059, p. 1121–1124, https://doi.org/10.1126/science.1210695
Haq, B. U., and Schutter, S. R., 2008, A chronology of Paleozoic sea-level changes: Science, v. 322, n. 5898, p. 64–68, https://doi.org/10.1126/science.1161648

Haq, B. U., Hardenbol, J., and Vail, P. R., 1987, Chronology of Fluctuating Sea Levels since the Triassic: Science, v. 235, n. 4793, p. 1156–1167, https://doi.org/10.1126/science.235.4793.1156
Hayes, J. M., Strauss, H., and Kaufman, A. J., 1999, The abundance of ^{13}C in marine organic matter and isotopic fractionation in the global biogeochemical cycle of carbon during the past 800 Ma: Chemical Geology, v. 161, n. 1–3, p. 103–125, https://doi.org/10.1016/S0009-2541(99)00083-2
Heim, N. A., Knope, M. L., Schaal, E. K., Wang, S. C., and Payne, J. L., 2015, Cope's rule in the evolution of marine animals: Science, v. 347, n. 6224, p. 867–870, https://doi.org/10.1126/science.1260065
Higgins, J. A., Fischer, W. W., and Schrag, D. P., 2009, Oxygenation of the ocean and sediments: Consequences for the seafloor carbonate factory: Earth and Planetary Science Letters, v. 284, n. 1–2, p. 25–33, https://doi.org/10.1016/j.epsl.2009.03.039
Holland, H. D., 1984, The chemical evolution of the atmosphere and oceans: New Jersey, Princeton University Press, 583 p.
Holser, W. T., Schidlowski, M., Mackenzie, F. T., and Maynard, J. B., 1988, Geochemical cycles of carbon and sulfur, *in* Gregor, C. B., Garrels, R. M., Mackenzie, T., and Maynard, J. B., editors, Chemical Cycles in the Evolution of the Earth: New York, John Wiley & Sons, p. 105–174.
Hönisch, B., Ridgwell, A., Schmidt, D. N., Thomas, E., Gibbs, S. J., Sluijs, A., Zeebe, R., Kump, L. R., Martindale, R. C., Greene, S. E., Kiessling, W., Ries, J., Zachos, J. C., Royer, D. L., Barker, S., Marchitto, T. M., Moyer, R., Pelejero, C., Ziveri, P., Foster, G. L., and Williams, B., 2012, The geological record of ocean acidification: Science, v. 335, n. 6072, p. 1058, https://doi.org/10.1126/science.1208277
Husson, J. M., and Peters, S. E., 2017, Atmospheric oxygenation driven by unsteady growth of the continental sedimentary reservoir: Earth and Planetary Science Letters, v. 460, p. 68–75, https://doi.org/10.1016/j.epsl.2016.12.012
Husson, J. M., Schoene, B., Bluher, S., and Maloof, A. C., 2016, Chemostratigraphic and U–Pb geochronologic constraints on carbon cycling across the Silurian–Devonian boundary: Earth and Planetary Science Letters, v. 436, p. 108–120, https://doi.org/10.1016/j.epsl.2015.11.044
Jenkyns, H. C., 1995, Carbon-isotope stratigraphy and paleoceanographic significance of the Lower Cretaceous shallow-water carbonates of Resolution Guyot, Mid-Pacific Mountains: Northwest Pacific atolls and guyots: Proceedings of the Ocean Drilling Program, Scientific results, v. 143, pages 99–104.
Knoll, A. H., Hayes, J. M., Kaufman, A. J., Swett, K., and Lambert, I. B., 1986, Secular variation in carbon isotope ratios from Upper Proterozoic successions of Svalbard and East Greenland: Nature, v. 321, n. 6073, p. 832–838, https://doi.org/10.1038/321832a0
Kump, L. R., 1991, Interpreting carbon-isotope excursions: Strangelove oceans: Geology, v. 19, n. 4, p. 299–302, https://doi.org/10.1130/0091-7613(1991)019<0299:ICIESO>2.3.CO;2
——— 1993, The coupling of the carbon and sulfur biogeochemical cycles over Phanerozoic time, *in* Wollast, R., Mackenzie, F. T., and Chou, L., editors, Interactions of C, N, P and S Biogeochemical Cycles and Global Change: NATO ASI Series I, v. 4, p. 475–490, https://doi.org/10.1007/978-3-642-76064-8_19
Kump, L. R., and Arthur, M. A., 1997, Global chemical erosion during the Cenozoic: Weatherability balances the budgets, *in* Ruddiman, W. F., editor, Tectonic Uplift and Climate Change: New York, Springer, p. 399–426, https://doi.org/10.1007/978-1-4615-5935-1_18
——— 1999, Interpreting carbon-isotope excursions: Carbonates and organic matter: Chemical Geology, v. 161, n. 1–3, p. 181–198, https://doi.org/10.1016/S0009-2541(99)00086-8
Kump, L. R., and Garrels, R. M., 1986, Modeling atmospheric O_2 in the global sedimentary redox cycle: American Journal of Science, v. 286, n. 5, p. 337–360, https://doi.org/10.2475/ajs.286.5.337
Laakso, T. A., and Schrag, D. P., 2014, Regulation of atmospheric oxygen during the Proterozoic: Earth and Planetary Science Letters, v. 388, p. 81–91, https://doi.org/10.1016/j.epsl.2013.11.049
Lasaga, A. C., 1980, The kinetic treatment of geochemical cycles: Geochimica et Cosmochimica Acta, v. 44, n. 6, p. 815–828, http://dx.doi.org/10.1016/0016-7037(80)90263-X
——— 1981, Dynamic treatment of geochemical cycles: Global kinetics, *in* Lasaga, A. C., and Kirkpatrick, R. J., editors, Kinetics of Geochemical Process: Reviews in Mineralogy, v. 8, p. 69–110.
——— 1989, A new approach to isotopic modeling of the variation of atmospheric oxygen through the Phanerozoic: American Journal of Science, v. 289, n. 4, p 411–435, https://doi.org/10.2475/ajs.289.4.411
Lasaga, A. C., and Ohmoto, H., 2002, The oxygen geochemical cycle: dynamics and stability: Geochimica et Cosmochimica Acta, v. 66, n. 3, p. 361–381, https://doi.org/10.1016/S0016-7037(01)00685-8
Lasaga, A. C., Berner, R. A., and Garrels, R. M., 1985, An improved geochemical model of atmospheric CO_2 fluctuations over the past 100 million years, *in* Sundquist, E. T., and Broecker, W. S., editors, The Carbon Cycle and Atmospheric CO_2: Natural Variations Archean to Present: Washington D. C., American Geophysical Union, Geophysical Monograph Series, v. 32, p. 397–411, https://doi.org/10.1029/GM032p0397
Lathi, B. P., 1992, Linear systems and signals: Carmichael, California, Berkeley-Cambridge Press, 656 p.
Lau, K. V., Maher, K., Altiner, D., Kelley, B. M., Kump, L. R., Lehrmann, D. J., Silva-Tamayo, J. C., Weaver, K. L., Yu, M., and Payne, J. L., 2016, Marine anoxia and delayed Earth system recovery after the end-Permian extinction: Proceedings of the National Academy of Sciences, v. 113, n. 9, p. 2360–2365, https://doi.org 10.1073/pnas.1515080113
Logan, G. A., Hayes, J. M., Hieshima, G. B., and Summons, R. E., 1995, Terminal Proterozoic reorganization of biogeochemical cycles: Nature, v. 376, n. 6535, p. 53–56, https://doi.org/10.1038/376053a0
Lyons, T. W., Reinhard, C. T., and Planavsky, N. J., 2014, The rise of oxygen in Earth's early ocean and atmosphere: Nature, v. 506, n. 7488, p. 307–315, https://doi.org/10.1038/nature13068
Magaritz, M., 1989, ^{13}C minima follow extinction events: A clue to faunal radiation: Geology, v. 17, n. 4, p. 337–340, https://doi.org/10.1130/0091-7613(1989)017<0337:CMFEEA>2.3.CO;2
Maloof, A. C., Porter, S. M., Moore, J. L., Dudás, F. Ö., Bowring, S. A., Higgins, J. A., Fike, D. A., and Eddy,

M. P., 2010, The earliest Cambrian record of animals and ocean geochemical change: Geological Society of America Bulletin, v. 122, n. 11–12, p. 1731–1774, https://doi.org/10.1130/B30346.1
McKenzie, N. R., Horton, B. K., Loomis, S. E., Stockli, D. F., Planavsky, N. J., and Lee, C.-T. A., 2016, Continental arc volcanism as the principal driver of icehouse-greenhouse variability: Science, v. 352, n. 6284, p. 444–447, https://doi.org/10.1126/science.aad5787
Meyer, K. M., Yu, M., Lehrmann, D., van de Schootbrugge, B., and Payne, J. L., 2013, Constraints on Early Triassic carbon cycle dynamics from paired organic and inorganic carbon isotope records: Earth and Planetary Science Letters, v. 361, p. 429–435, https://doi.org/10.1016/j.epsl.2012.10.035
Meyer, K. M., Ridgwell, A., and Payne, J. L., 2016, The influence of the biological pump on ocean chemistry: Implications for long-term trends in marine redox chemistry, the global carbon cycle, and the evolution of marine animal ecosystems: Geobiology, v. 14, n. 3, p. 207–219, https://doi.org/10.1111/gbi.12176
Meyers, S. R., and Peters, S. E., 2011, A 56 million year rhythm in north american sedimentation during the Phanerozoic: Earth and Planetary Science Letters, v. 303, n. 3–4, p. 174–180, https://doi.org/10.1016/j.epsl.2010.12.044
Milliman, J. D., 1993, Production and accumulation of calcium carbonate in the ocean: Budget of a nonsteady state: Global Biogeochemical Cycles, v. 7, v. 4, p. 927–957, https://doi.org/10.1029/93GB02524
Oehlert A. M., and Swart. P. K., 2014, Interpreting carbonate and organic carbon isotope covariance in the sedimentary record: Nature Communications, v. 5, p. 4672, https://doi.org/10.1038/ncomms5672
Parente, M., Frijia, G., and Lucia, M. Di, 2007, Carbon-isotope stratigraphy of Cenomanian–Turonian platform carbonates from the southern Apennines (Italy): a chemostratigraphic approach to the problem of correlation between shallow-water and deep-water successions: Journal of the Geological Society, v. 164, n. 3, p. 609–620, https://doi.org/10.1144/0016-76492006-010
Payne, J. L., Lehrmann, D. J., Wei, J., Orchard, M. J., Schrag, D. P., and Knoll, A. H., 2004, Large perturbations of the carbon cycle during recovery from the End-Permian extinction: Science, v. 305, n. 5683, p. 506–509, https://doi.org/10.1126/science.1097023
Peters, S. E., 2007, The problem with the Paleozoic: Paleobiology, v. 33, n. 2, p. 165–181, https://doi.org/10.1666/06067.1
——— 2008, Macrostratigraphy and its promise for paleobiology: Paleontological Society Papers, v. 14, p. 205–232.
Peters, S. E., and Gaines, R. R., 2012, Formation of the Great Unconformity as a trigger for the Cambrian explosion: Nature, v. 484, n. 7394, p. 363–366, https://doi.org/10.1038/nature10969
Pollard, D., Kump, L., and Zachos, J., 2013, Interactions between carbon dioxide, climate, weathering, and the Antarctic ice sheet in the earliest Oligocene: Global and Planetary Change, v. 111, p. 258–267, https://doi.org/10.1016/j.gloplacha.2013.09.012
Price, G. D., Főzy, I., and Pálfy, J., 2016, Carbon cycle history through the Jurassic–Cretaceous boundary: A new global $\delta^{13}C$ stack: Palaeogeography, Palaeoclimatology, Palaeoecology, v. 451, p. 46–61, https://doi.org/10.1016/j.palaeo.2016.03.016
Raup, D. M., and Sepkoski, J. J., Jr., 1982, Mass extinctions in the marine fossil record: Science, v. 215, n. 4539, p. 1501–1503, https://doi.org/10.1126/science.215.4539.1501
Redfield. A. C., 1958, The biological control of chemical factors in the environment: American Scientist, v. 46, n. 3, p. 205–221, http://www.jstor.org/stable/27827150
Reinhard, C. T., Planavsky, N. J., Gill, B. C., Ozaki, K., Robbins, L. J., Lyons, T. W., Fischer, W. W., Wang, C., Cole, D. B., and Konhauser, K. O., 2017, Evolution of the global phosphorus cycle: Nature, v. 541, n. 7637, p. 386–389, https://doi.org/10.1038/nature20772
Ridgwell, A., and Zeebe, R. E., 2005, The role of the global carbonate cycle in the regulation and evolution of the Earth system: Earth and Planetary Science Letters, v. 234, n. 3–4, p. 299–315, https://doi.org/10.1016/j.epsl.2005.03.006
Rohde, R. A., and Muller, R. A., 2005, Cycles in fossil diversity: Nature, v. 434, n. 7030, p. 208–210, https://doi.org/10.1038/nature03339
Sarmiento, J. L., and Gruber, N., 2006, Ocean biogeochemical dynamics: Princeton, New Jersey, Princeton University Press, 528 p.
Saitoh, M., Ueno, Y., Isozaki, Y., Shibuya, T., Yao, J., Ji, Z., Shozugawa, K., Matsuo, M., and Yoshida. N., 2015, Authigenic carbonate precipitation at the end-Guadalupian (middle Permian) in China: Implications for the carbon cycle in ancient anoxic oceans: Progress in Earth and Planetary Science, v. 2, n. 1, p. 41, https://doi.org/10.1186/s40645-015-0073-2
Saltzman, M. R., 2005, Phosphorus, nitrogen, and the redox evolution of the Paleozoic oceans: Geology, v. 33, n. 7, p. 573–576, https://doi.org/10.1130/G21535.1
Saltzman, M. R., and Thomas, E., 2012, Carbon Isotope Stratigraphy, *in* Gradstein, F., Ogg, J., Ogg, G., and Schmitz, M., editors, The Geologic Timescale 2012: Amsterdam, Elsevier, p. 207–233.
Saltzman, M. R., Young, S. A., Kump, L. R., Gill, B. C., Lyons, T. W., and Runnegar, B., 2011, Pulse of atmospheric oxygen during the late Cambrian: Proceedings of the National Academy of Sciences of the United States of America, v. 108, n. 10, p. 3876–3881, https://doi.org/10.1073/pnas.1011836108
Scholle, P. A., and Arthur, M. A., 1980, Carbon isotope fluctuations in Cretaceous pelagic limestones: Potential stratigraphic and petroleum exploration tool: AAPG Bulletin, v. 64, n. 1, p. 67–87.
Schrag, D. P., Higgins, J. A., Macdonald, F. A., and Johnston, D. T., 2013, Authigenic Carbonate and the History of the Global Carbon Cycle: Science, v. 339, n. 6119, p. 540–543, https://doi.org/10.1126/science.1229578
Sekine, Y., Tajika, E., Ohkouchi, N., Ogawa, N. O., Goto, K., Tada, R., Yamamoto, S., and Kirschvink, J. L., 2010, Anomalous negative excursion of carbon isotope in organic carbon after the last Paleoproterozoic glaciation in North America: Geochemistry, Geophysics, Geosystems, v. 11, n. 8, p. Q08019, https://doi.org/10.1029/2010GC003210

Shibuya, T., Tahata, M., Kitajima, K., Ueno, Y., Komiya, T., Yamamoto, S., Igisu, M., Terabayashi, M., Sawaki, Y., Takai, K., Yoshida, N., and Maruyama, S., 2012, Depth variation of carbon and oxygen isotopes of calcites in Archean altered upper oceanic crust: Implications for the CO_2 flux from ocean to oceanic crust in the Archean: Earth and Planetary Science Letters, v. 321–322, p. 64–73, https://doi.org/10.1016/j.epsl.2011.12.034

Sloss, L. L., 1963, Sequences in the cratonic interior of north america: Geological Society of America Bulletin, v. 74, n. 2, p. 93–114, https://doi.org/10.1130/0016-7606(1963)74[93:SITCIO]2.0.CO;2

Southam, J. R., and Hay, W. W., 1976, Dynamical formulation of Broecker's model for marine cycles of biologically incorporated elements: Journal of the International Association for Mathematical Geology, v. 8, n. 5, p. 511–527, https://doi.org/10.1007/BF01042991

Sun, X., and Turchyn, A. V., 2014, Significant contribution of authigenic carbonate to marine carbon burial: Nature Geoscience, v. 7, n. 3, p. 201–204, https://doi.org/10.1038/ngeo2070

Sun, Y., Joachimski, M. M., Wignall, P. B., Yan, C., Chen, Y., Jiang, H., Wang, L., and Lai, X., 2012, Lethally hot temperatures during the Early Triassic greenhouse: Science, v. 338, n. 6105, p. 366–370, https://doi.org/10.1126/science.1224126

Svensen, H., Planke, S., Malthe-Sørenssen, A., Jamtveit, B., Myklebust, R., Eidem, T. R., and Rey, S. S., 2004, Release of methane from a volcanic basin as a mechanism for initial Eocene global warming: Nature, v. 429, n. 6991, p. 542–545, https://doi.org/10.1038/nature02566

Svensen, H., Planke, S., Chevallier, L., Malthe-Sørenssen, A., Corfu, F., and Jamtveit, B., 2007, Hydrothermal venting of greenhouse gases triggering Early Jurassic global warming: Earth and Planetary Science Letters, v. 256, n. 3–4, p. 554–566, http://dx.doi.org/10.1016/j.epsl.2007.02.013

Svensen, H., Planke, S., Polozov, A. G., Schmidbauer, N., Corfu, F., Podladchikov, Y. Y., and Jamtveit, B., 2009, Siberian gas venting and the end-permian environmental crisis: Earth and Planetary Science Letters, v. 277, n. 3–4, p. 490–500, https://doi.org/10.1016/j.epsl.2008.11.015

Swart, P. K., 2008, Global synchronous changes in the carbon isotopic composition of carbonate sediments unrelated to changes in the global carbon cycle: Proceedings of the National Academy of Sciences of the United States of America, v. 105, n. 37, p. 13741–13745, https://doi.org/10.1073/pnas.0802841105

Swart, P. K., and Eberli, G., 2005, The nature of the $\delta^{13}C$ of periplatform sediments: Implications for stratigraphy and the global carbon cycle: Sedimentary Geology, v. 175, n. 1–4, p. 115–129, https://doi.org/10.1016/j.sedgeo.2004.12.029

Swart, P. K., and Kennedy, M. J., 2012, Does the global stratigraphic reproducibility of $\delta^{13}C$ in Neoproterozoic carbonates require a marine origin? A Pliocene–Pleistocene comparison: Geology, v. 40, n. 1, p. 87–90, https://doi.org/10.1130/G32538.1

Thomazo, C., Vennin, E., Brayard, A., Bour, I., Mathieu, O., Elmeknassi, S., Olivier, N., Escarguel, G., Bylund, K. G., Jenks, J., Stephen, D. A., and Fara, E., 2016, A diagenetic control on the Early Triassic Smithian–Spathian carbon isotopic excursions recorded in the marine settings of the Thaynes Group (Utah, USA): Geobiology, v. 14, n. 3, p. 220–236, https://doi.org/10.1111/gbi.12174

Tziperman, E., Halevy, I., Johnston, D. T., Knoll, A. H., and Schrag, D. P., 2011, Biologically induced initiation of Neoproterozoic snowball-Earth events: Proceedings of the National academy of Sciences of the United States of America, v. 108, n. 37, p. 15091–15096, https://doi.org/10.1073/pnas.1016361108

Van Cappellen, P., and Ingall, E. D., 1996, Redox stabilization of the atmosphere and oceans by phosphorus-limited marine productivity: Science, v. 271, n. 5248, p. 493, https://doi.org/10.1126/science.271.5248.493

Veizer, J., Holser, W. T., and Wilgus, C. K., 1980, Correlation of $^{13}C/^{12}C$ and $^{34}S/^{32}S$ secular variations: Geochimica et Cosmochimica Acta, v. 44, n. 4, p. 579–587, https://doi.org/10.1016/0016-7037(80)90250-1

Veizer, J., Ala, D., Azmy, K., Bruckschen, P., Buhl, D., Bruhn, F., Giles, C. A. F., Diener, A., Ebneth, S., Godderis, Y., Jasper, T., Korte, C., Pawellek, F., Polaha, O. G., and Strauss, H., 1999, $^{87}Sr/^{86}Sr$, $\delta^{13}C$ and $\delta^{18}O$ evolution of Phanerozoic seawater: Chemical Geology, v. 161, n. 1–3, p. 59–88, http://dx.doi.org/10.1016/S0009-2541(99)00081-9

Vincent, B., van Buchem, F. S., Bulot, L. G., Immenhauser, A., Caron, M., Baghbani, D., and Huc, A. Y., 2010, Carbon-isotope stratigraphy, biostratigraphy and organic matter distribution in the Aptian–Lower Albian successions of southwest Iran (Dariyan and Kazhdumi formations): GeoArabia Special Publication, v. 4, n. 1, p. 139–197.

Wallmann, K., 2014, Is late Quaternary climate change governed by self-sustained oscillations in atmospheric CO_2?: Geochimica et Cosmochimica Acta, v. 132, p. 413–439, https://doi.org/10.1016/j.gca.2013.10.046

Walker, J. C. G., Hays, P. B., and Kasting, J. F., 1981, A negative feedback mechanism for the long-term stabilization of Earth's surface temperature: Journal of Geophysical Research: Oceans, v. 86, n. C10, p. 9776–9782, https://doi.org/10.1029/JC086iC10p09776

Wignall, P. B., 2001, Large igneous provinces and mass extinctions: Earth-Science Reviews, v. 53, n. 1–2, p. 1–33, https://doi.org/10.1016/S0012-8252(00)00037-4

Wildman, R. A., Berner, R. A., Petsch, S. T., Bolton, E. W., Eckert, J. O., Mok, U., and Evans, J. B., 2004, The weathering of sedimentary organic matter as a control on atmospheric O_2: I. analysis of a black shale: American Journal of Science, v. 304, n. 3, p. 234–249, https://doi.org/10.2475/ajs.304.3.234

Worsley, T. R., Nance, D., and Moody, J. B., 1984, Global tectonics and eustasy for the past 2 billion years: Marine Geology, v. 58, n. 3–4, p. 373–400, https://doi.org/10.1016/0025-3227(84)90209-3

Zachos, J. C., and Kump, L. R., 2005, Carbon cycle feedbacks and the initiation of Antarctic glaciation in the earliest Oligocene: Global and Planetary Change, v. 47, n. 1, p. 51–66, https://doi.org/10.1016/j.gloplacha.2005.01.001

Zachos, J. C., Pagani, M., Sloan, L., Thomas, E., and Billups, K., 2001, Trends, rhythms, and aberrations in global climate 65 Ma to present: Science, v. 292, n. 5517, p. 686–693, https://doi.org/10.1126/science.1059412

Zhou, C., Guan, C., Cui, H., Ouyang, Q., and Wang, W., 2016, Methane-derived authigenic carbonate from the lower Doushantuo formation of South China: Implications for seawater sulfate concentration and global carbon cycle in the early Ediacaran ocean: Palaeogeography, Palaeoclimatology, Palaeoecology, v. 461, p. 145–155, https://doi.org/10.1016/j.palaeo.2016.08.017